NAVAL POSTGRADUATE SCHOOL

MONTEREY, CALIFORNIA

THESIS

COLD SPRAY OF FUNCTIONALLY GRADED ALUMINUM METAL MATRIX COMPOSITE COATINGS REINFORCED WITH BORON CARBIDE AND BORON NITRIDE NANOTUBES

by

Richard L. Schmidt

December 2023

Thesis Advisor: Troy Ansell
Second Reader: Young W. Kwon

THIS PAGE INTENTIONALLY LEFT BLANK

REPORT DOCUMENTATION PAGE	*Form Approved OMB No. 0704-0188*

1. AGENCY USE ONLY *(Leave blank)*	**2. REPORT DATE** December 2023	**3. REPORT TYPE AND DATES COVERED** Master's thesis

4. TITLE AND SUBTITLE
COLD SPRAY OF FUNCTIONALLY GRADED ALUMINUM METAL MATRIX COMPOSITE COATINGS REINFORCED WITH BORON CARBIDE AND BORON NITRIDE NANOTUBES

5. FUNDING NUMBERS

6. AUTHOR(S) Richard L. Schmidt

7. PERFORMING ORGANIZATION NAME(S) AND ADDRESS(ES)
Naval Postgraduate School
Monterey, CA 93943-5000

8. PERFORMING ORGANIZATION REPORT NUMBER

9. SPONSORING / MONITORING AGENCY NAME(S) AND ADDRESS(ES)
N/A

10. SPONSORING / MONITORING AGENCY REPORT NUMBER

11. SUPPLEMENTARY NOTES The views expressed in this thesis are those of the author and do not reflect the official policy or position of the Department of Defense or the U.S. Government.

12a. DISTRIBUTION / AVAILABILITY STATEMENT
Approved for public release. Distribution is unlimited.

12b. DISTRIBUTION CODE
A

13. ABSTRACT (maximum 200 words)

Aluminum 7075 alloys are extensively utilized in the aerospace industry for their relatively high specific strength coupled with decent corrosion resistance and cost-effectiveness. Being an Al alloy, however, the material suffers from low wear resistance. Cold gas dynamic spray, commonly known as cold spray, is a thermal spray technique applicable for on-site repair of metallic surfaces, particularly Al, as well as coating onto Al substrates to enhance wear resistance among other properties. Improving the wear resistance of Al requires the integration of a reinforcing filler/s. Notably, there is a research gap regarding the cold spray application of compositionally graded, dual-reinforced aluminum metal matrix composites (Al-MMC).

In this study, aircraft-grade aluminum (Al7075) underwent the cold spray process with reinforcement from boron carbide (B4C) and boron nitride nanotubes (BNNT). The creation of a functionally graded coating (FGC) was achieved through high-energy ball milling, incorporating varying compositions of 10, 15, and 20 vol.% µB4C. This coating included a top layer with 2 vol.% BNNT and 2 vol.% nB4C. Comparative assessments of the different coating layers were conducted, with a specific focus on evaluating their subsequent wear resistance. Remarkably, all µB4C compositions exhibited sustained or enhanced wear resistance, despite experiencing low deposition rates, especially in the layers containing 2 vol.% BNNT and 2 vol.% nB4C.

14. SUBJECT TERMS cold spray, boron carbide, BNNT, boron nitride nanotubes, 7075	**15. NUMBER OF PAGES** 93
	16. PRICE CODE

17. SECURITY CLASSIFICATION OF REPORT	**18. SECURITY CLASSIFICATION OF THIS PAGE**	**19. SECURITY CLASSIFICATION OF ABSTRACT**	**20. LIMITATION OF ABSTRACT**
Unclassified	Unclassified	Unclassified	UU

NSN 7540-01-280-5500

Standard Form 298 (Rev. 2-89)
Prescribed by ANSI Std. 239-18

THIS PAGE INTENTIONALLY LEFT BLANK

Approved for public release. Distribution is unlimited.

COLD SPRAY OF FUNCTIONALLY GRADED ALUMINUM METAL MATRIX COMPOSITE COATINGS REINFORCED WITH BORON CARBIDE AND BORON NITRIDE NANOTUBES

Richard L. Schmidt
Lieutenant, United States Navy
BSAST, Thomas A Edison State College, 2010

Submitted in partial fulfillment of the
requirements for the degree of

MASTER OF SCIENCE IN AEROSPACE ENGINEERING

from the

NAVAL POSTGRADUATE SCHOOL
December 2023

Approved by: Troy Ansell
Advisor

Young W. Kwon
Second Reader

Brian S. Bingham
Chair, Department of Mechanical and Aerospace Engineering

THIS PAGE INTENTIONALLY LEFT BLANK

ABSTRACT

Aluminum 7075 alloys are extensively utilized in the aerospace industry for their relatively high specific strength coupled with decent corrosion resistance and cost-effectiveness. Being an Al alloy, however, the material suffers from low wear resistance. Cold gas dynamic spray, commonly known as cold spray, is a thermal spray technique applicable for on-site repair of metallic surfaces, particularly Al, as well as coating onto Al substrates to enhance wear resistance among other properties. Improving the wear resistance of Al requires the integration of a reinforcing filler/s. Notably, there is a research gap regarding the cold spray application of compositionally graded, dual-reinforced aluminum metal matrix composites (Al-MMC).

In this study, aircraft-grade aluminum (Al7075) underwent the cold spray process with reinforcement from boron carbide (B4C) and boron nitride nanotubes (BNNT). The creation of a functionally graded coating (FGC) was achieved through high-energy ball milling, incorporating varying compositions of 10, 15, and 20 vol.% μB4C. This coating included a top layer with 2 vol.% BNNT and 2 vol.% nB4C. Comparative assessments of the different coating layers were conducted, with a specific focus on evaluating their subsequent wear resistance. Remarkably, all μB4C compositions exhibited sustained or enhanced wear resistance, despite experiencing low deposition rates, especially in the layers containing 2 vol.% BNNT and 2 vol.% nB4C.

THIS PAGE INTENTIONALLY LEFT BLANK

TABLE OF CONTENTS

LIST OF FIGURES

THIS PAGE INTENTIONALLY LEFT BLANK

LIST OF TABLES

THIS PAGE INTENTIONALLY LEFT BLANK

LIST OF ACRONYMS AND ABBREVIATIONS

Al7075	aluminum 7075 alloy
ARL	Army Research Laboratory
ASTM	American Society for Testing and Materials
BNNB	boron nitride nanobarb
BNNT	boron nitride nanotubes
BPR	ball to powder ratio
CGSM	cold gas-dynamic spray
CNT	carbon nanotubes
COF	coefficient of friction
DE	deposition efficiency
EDS	energy dispersive x-ray spectroscopy
FGC	functional graded coating
He	helium
HEBM	high energy ball mill
HPCS	high pressure cold spray
HVOF	high velocity oxy-fuel
LPCS	low pressure cold spray
MMC	metal matrix composite
N_2	nitrogen gas
Ra	arithmetical average roughness
RMS	root mean square roughness
RPM	revolutions per minute
SEM	scanning electron microscope
SS	stainless steel
Vol.%	volume percentage

THIS PAGE INTENTIONALLY LEFT BLANK

ACKNOWLEDGMENTS

I must acknowledge the exceptional guidance provided by my thesis advisor, Professor Troy Ansell. His expertise, patience, and commitment to my academic growth have been instrumental in shaping my research and overall approach. The insightful feedback and mentorship he provided were invaluable, and I am profoundly thankful for his support over the last year.

I am equally indebted to Achyuth Kulkarni, whose remarkable expertise and invaluable assistance left an indelible mark on the technical aspects of my thesis. Whether it was cold spraying or countless hours executing profilometry, he consistently went above and beyond to ensure the seamless and efficient execution of my research.

Furthermore, I would like to acknowledge the contributions of Kenneth Silim and Sneha Gokaraju, who interned at NPS over the summer. Their early work on optimizing parameters and powders for cold spray provided a strong foundation for my research. Additionally, I extend my appreciation to Professor Young Kwon for being my second reader and Professor Chanman Park for providing invaluable assistance in material analysis and preparation.

Lastly, my deepest appreciation goes to my parents. Their unending encouragement, selfless sacrifices, and unwavering belief in my abilities have been an enduring source of motivation throughout this challenging journey. They have been a pillar of support, offering both emotional sustenance and understanding during the most demanding moments of this thesis. I am eternally grateful for their steadfast faith in my aspirations.

THIS PAGE INTENTIONALLY LEFT BLANK

I. INTRODUCTION

A. MOTIVATION

Aluminum 7075 (Al7075) is an aluminum alloy utilized in both commercial and military aircraft structures. With any aircraft comes the repair process and extensions to an aircraft life cycle have become more common over the years. When an aluminum structural component is damaged, it is often removed and sent back to either an intermediate or depot level facility for repair. The amount of time for the removal and replacement of a substitute part can account for many man-hours at the organizational level. What if, however, the component could be repaired or replaced without even removing it? A relatively new process called cold spray may be a technique that could be used by a Sailor or Marine to keep asset readiness at acceptable levels even while deployed in logistically constrained theaters of operation.

Cold gas dynamic spray, cold spray for short, is a thermal spray technique for applying relatively thick metal or metal composite coatings onto a substrate. Unlike the more familiar thermal spray methods like plasma spray or high velocity oxygen fuel (HVOF), cold spray does not require melting of precursor powders before spraying. As a result, post-spray residual strain is mitigated, and deleterious secondary phase formation is avoided. Furthermore, composite coatings consisting of nanoparticles like carbon nanotubes or boron nitride nanotubes could be sprayed with the risk of oxidation that occurs at the elevated temperatures seen in plasma spray or HVOF. By incorporating nano- and micro-particles in the mixture (known as coating reinforcement), a repair could be made that is more wear and corrosion resistant than the surrounding structure in which the repair was made.

Since cold spray operates at much lower temperatures, it is possible to conduct a repair in place without significantly affecting the surrounding components. So, in certain cases, cold spray deposits could replace welding repairs. This can reduce labor and can lead to a longer lasting repair. The cold spray technique is portable. Plasma spray and HVOF, for example, could not be portable due to gas, electrical, and thermal requirements.

These requirements are not as limiting for cold spray as a Sailor, or Marine, would only need a source of compressed air and standard power access. Furthermore, recent developments have allowed the technique to be used to "print" free-standing objects from a digital model much like 3D-printers based on laser powder bed fusion (LPBF) or fused filament fabrication (FFF) for 3D-plastic printing. This makes cold spray very desirable as a technique for component replacement while deployed.

Despite the advantages of cold spray, some challenges remain like spraying of composite and/or functionally graded coatings. A cold spray deposit is formed by accelerating particles to a critical velocity, which then impacts a substrate with sufficient energy to adhere to the substrate. This process necessarily requires particles to undergo severe plastic deformation upon impact. Metals like Al or copper (Cu) exhibit sufficient ductility to be sprayed. Harder ceramic particles do not often fracture before yielding, i.e., brittle fracture. This limits the amount of ceramic phase that can be cold sprayed. Additionally, nanoparticles used as reinforcing (e.g., improvements to adhesion strength) fillers in composite coatings are also limited due to the high particle speeds achievable, which could lead to erosion of the substrate as opposed to adhesion. Nanoparticles also typically exhibit poor flowability invariably leading to clogged powder lines and nozzles. For a functionally graded coating, where adhesion and wear resistance improvements are sought, both ceramic and nanoparticle fillers are needed but optimization is required for adequate coating deposition.

B. OBJECTIVES

The aim of this study was to increase the boron carbide ceramic particulate content in the surface layers of an aluminum metal matrix composite (MMC) when applied to an Al7075 substrate. This was to increase the hardness and wear resistance of the Al-MMC. To accomplish increasing ceramic inclusions, a novel aluminum composite powder had to be developed and applied through a low-pressure cold spray process.

Boron carbide (B_4C) is increasingly utilized as a ceramic reinforcement in aluminum due to its hardness and high melting temperature, which complements the relatively soft aluminum without adding significant weight. Another ceramic gaining

popularity is boron nitride nanotubes (BNNT), known for their structural similarities to carbon nanotubes and greater durability. By incorporating these ceramic phases into an MMC and adjusting their volume percentages, improved properties, including enhanced hardness and wear resistance, can be achieved.

THIS PAGE INTENTIONALLY LEFT BLANK

II. BACKGROUND

A. COLD SPRAY OVERVIEW

The cold spray method is a material deposition process that involves accelerating solid particles to supersonic speeds. After impacting onto a substrate, the particles form a dense, cohesive coating without the need for melting like in plasma spray [1]. This process originated in the 1980s during supersonic wind tunnel testing conducted by Dr. Antolii Papyrin and his colleagues at the Russian Academy of Science [2]. They achieved this by utilizing a convergent-divergent de Laval-type nozzle [3], which allowed them to coat ductile materials, from a powder feedstock, and spraying without significantly increasing their temperature [4]. Figure 1 shows a schematic diagram of the spray and adhesion processes involved [5].

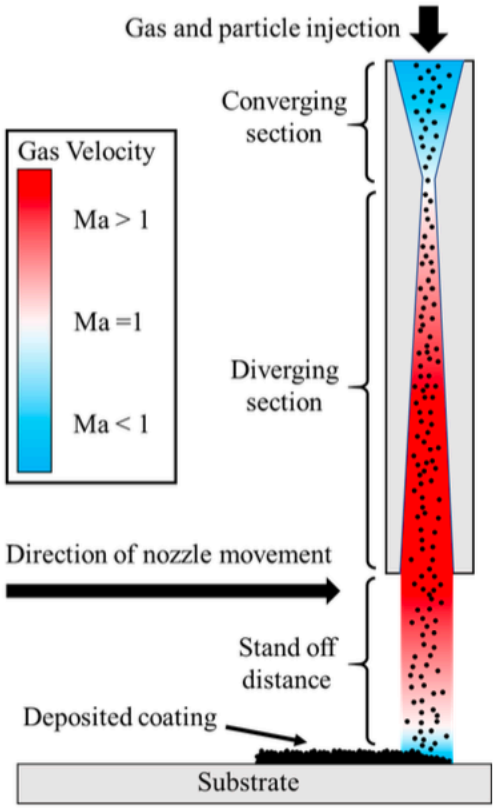

Figure 1. Cold spray diagram. Source: [5].

Cold spray deposition distinguishes itself from other thermal spray techniques by avoiding the particle melting process, remaining a solid-state deposition method [6]. The temperature of the plume at the nozzle's end is notably lower when compared to other thermal spray applications [7]. In cold spray, temperatures are maintained below 800°C, as opposed to the HVOF thermal spray, which can reach temperatures as high as 3000°C [8]. As seen in Figure 2, the differences in particle velocity and temperature in regards to the different thermal spray techniques is shown.

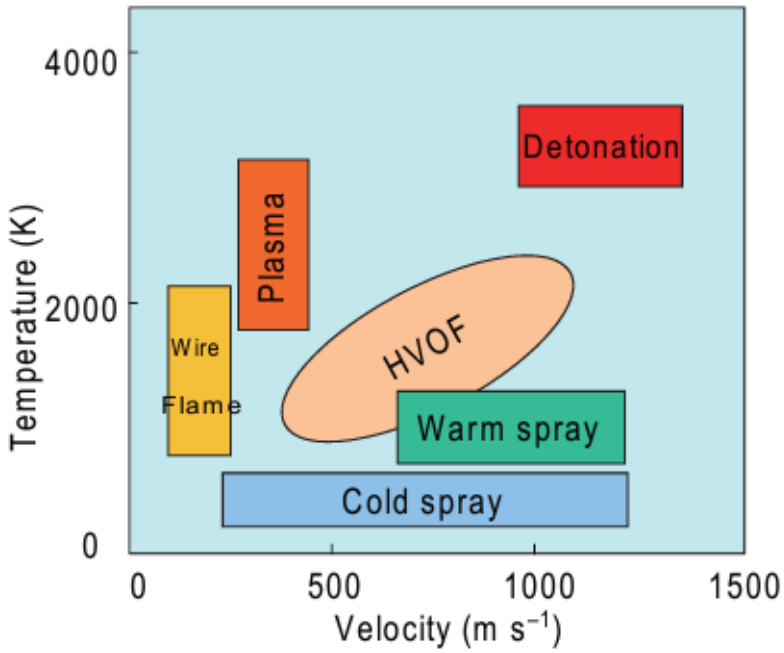

Figure 2. Comparison of various thermal spray processes. Source: [9].

Warm spray, while having temperatures near the powder's melting point during spraying, shares a common requirement with cold spray, necessitating high powder velocity for impact bonding [9]. The defining feature of cold spray deposition lies in the unique adhesion mechanism of powder particles to the substrate or base material. This process relies solely on the kinetic energy of the particles (see Figure 3), causing plastic deformation upon impact [8]. It is proposed that the bonding mechanism is thought to result from an adiabatic shear instability at the interface during impact [10]. This instability arises due to high strain rate deformation processes and creates a fast outward-moving jet of

material that acts in a viscous-like manner [11]. This metal jet also serves as a means of removing the oxide layer allowing for true metal to metal contact in the process [10].

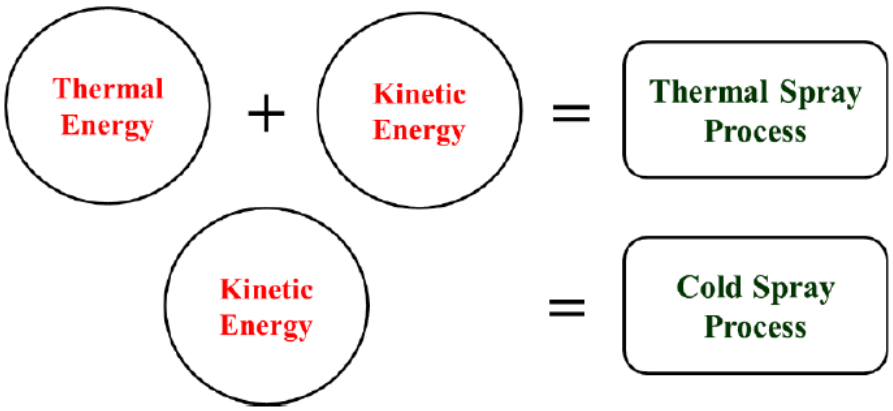

Figure 3. Sources of energy in a conventional thermal spray vs. cold gas dynamic spray process. Source: [8].

Cold spray technology can be categorized into two main types: low pressure cold spray (LPCS) and high-pressure cold spray (HPCS) systems (schematics shown in Figure 4). In HPCS systems, a lightweight carrier gas like nitrogen (N_2) or helium (He) is employed at higher pressure (580 psig) and temperature (800°C) [12]. The powder is introduced before the spray nozzle throat and is typically limited to denser pure metal particles or various alloys. On the other hand, LPCS systems are designed for lighter-weight powder particles, often consisting of metallic and ceramic powder blends. In LPCS, the powder mixture is injected into the divergent zone of the nozzle assembly, utilizing the carrier gas at lower pressures and temperatures (< 650°C) [12].

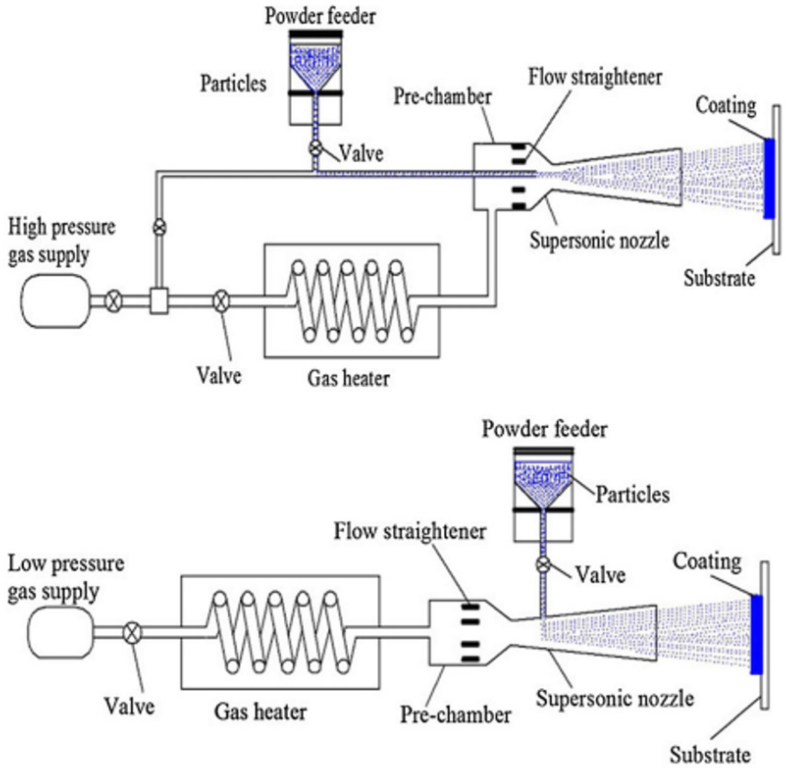

Figure 4. HPCS (top) and LPCS (bottom) schematic. Source: [13].

B. AIRCRAFT REPAIR

Cold spray technology is already making significant strides in the aviation industry, particularly in the repair and reconstruction of damaged aluminum alloy components. The U.S. Army Research Laboratory (ARL) Center for Cold Spray has demonstrated successful repairs on magnesium components of aircraft, showcasing the versatility and applicability of this innovative technique [14]. Cold spray offers distinct advantages over welding and lasers in this case. These advantages stem from the minimal thermal input, which avoids microstructural changes in the base alloy, and the low compressive residual stress when applied [15].

One key feature of cold spray is its ability to apply both thin and thick coatings, a flexibility that depends on various factors including temperature, pressure, size, and carrier gas requirements to propel the powder particles at the necessary velocity. If a thicker

coating is required, it can be achieved by applying multiple passes, offering a practical solution for a range of applications. In comparison to the traditional thermal spray process, cold spray stands out as a more cost-effective option. It demands lower initial investment, making it an attractive choice for industries seeking cost-efficient solutions [16]. Another notable advantage of cold spray is its ability to minimize porosity in the coatings. This is achieved because the powdered material never reaches its melting point during the spraying process. As a result, the risk of oxidation forming while the spraying is significantly reduced, contributing to the high quality and durability of the coatings [17].

Cold spray technology is making advances in the aviation industry, offering alternative repair and reconstruction options compared to welding or laser melting for aluminum alloy and magnesium components. Its adaptability in applying coatings of varying thickness, cost-effectiveness, and ability to minimize porosity make it a promising choice for various industrial applications.

C. ADHESION

Deposition efficiency (DE) primarily depends on the powder particles reaching their critical velocity. Once this velocity is attained, the particles will undergo deformation upon contact, forging a solid-state mechanical bond with either the substrate or other particles deposited during the cold spray process [18]. Particles deform plastically when their velocity exceeds the critical threshold; below this threshold, particles may either rebound or cause erosion [19]. In cold spray applications, only those particles surpassing or meeting the critical velocity threshold can actively contribute to the coating buildup or deposition as seen in Figure 5 [20].

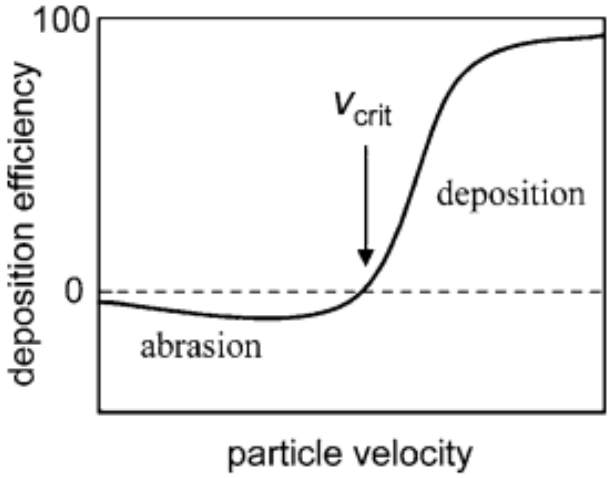

Figure 5. Particle velocity and DE correlation. Source: [21].

The attainment of critical velocity is contingent on multiple factors, encompassing the selection of the carrier gas, gas temperature, gas pressure, particle attributes (size, shape, and density), and the properties of the sprayed substrate [6]. The choice of carrier gas significantly impacts deposition efficiency and the ability of particulates to reach critical velocity, particularly in a LPCS application. Some combination of these parameters will affect the particle velocity and for every combination of powder/substrate, there exists an optimal range of particle velocities. Figure 6 shows these optimal velocities as a function of the particle impact temperature. If the particle velocities are too high, erosion of the substrate surface instead of adhesion will occur.

Commonly used carrier gases in cold spray include N_2, He, as well as compressed air. Helium, with its lower atomic mass, can attain much higher gas velocities than nitrogen (N_2), which is a naturally occurring diatomic molecule found in both the atmosphere and commercially compressed gas cylinders. This results in more efficient particle acceleration, leading to coatings with superior adhesion and reduced porosity [22]. Additionally, He is an inert gas, which means it does not chemically react with the sprayed particles, reducing the risk of oxidation. He does come at a cost as it is significantly more expensive than N_2, and there are concerns about its limited supply, making it less sustainable in the long term [23].

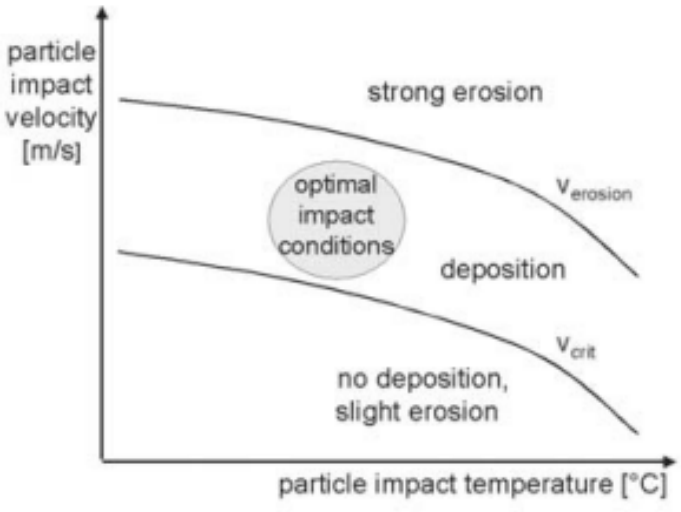

Figure 6. Correlation between impact velocity and temperature. Source: [24].

In contrast, N_2 is a cost-effective and readily available carrier gas. Gas prices fluctuate daily, but the cost of N_2 is around $0.30 per cubic foot while He is $1.82 per cubic foot. It is environmentally friendly, as it is abundant in the Earth's atmosphere and does not pose any toxicity or flammability concerns. However, due to its higher atomic mass, N_2 offers lower gas velocities compared to He, which can impact the efficiency of particle acceleration and bonding [22]. Coatings produced with N_2, as the carrier gas, may exhibit lower adhesion and increased porosity making it less suitable for applications where the highest coating quality is critical.

Ways of improving adhesion (and by extension, deposition efficiency) include feedstock preheating, surface preparation prior to spraying, and powder compositing. By preheating the feedstock powder prior to spraying, there is the potential to enhance deposition efficiency and reduce the required critical velocity. In a study conducted with copper powder in an LPCS process, two distinct batches were subjected to preheating at temperatures of 390°C and 500°C for one hour under vacuum conditions [25]. The results revealed a noteworthy 10% improvement in deposition efficiency for the batch preheated at 500°C. This enhancement can be attributed to a reduction in the microhardness of the

particles during the annealing process, ultimately facilitating improved deposition efficiency.

D. ALUMINUM METAL MATRIX COMPOSITES

Metal matrix composites (MMCs) are engineered materials consisting of a metal matrix reinforced with non-metallic or metallic phases [26]. These composites have gained significant attention in recent years due to their superior mechanical properties, wear resistance, and thermal stability [27]. MMCs have found applications in aerospace, automotive, and industrial sectors due to their exceptional wear resistance [28]. In aerospace specifically, MMCs are used for components subjected to extreme conditions, such as turbine blades and wear-resistant coatings.

MMCs with ceramic reinforcements have the potential to improve the mechanical properties of metals without increasing the weight or density [29] and are known for their higher modulus, hardness, and strength properties [30]. The hardness of MMCs is often higher than that of monolithic metals due to the presence of hard reinforcement phases. This increased hardness enhances resistance to abrasive wear, a critical consideration in various applications. The microstructure of MMCs plays a significant role in wear resistance. A uniform dispersion of reinforcement phases in the matrix improves wear resistance by reducing the potential for localized wear. The friction coefficient between the composite and the base matrix material influences wear rates. Low friction coefficients can minimize abrasive wear and reduce heat generation, resulting in lower wear rates.

Al7075 (Table 1 lists the composition of Al7075) is known for its mechanical properties, specifically fatigue resistance, and versatility in applications. A selection of important properties are listed in Table 2. This high-strength aluminum alloy has gained widespread usage in aircraft structures, including wings and stabilizers, owing to its lightweight nature and impressive strength-to-weight ratio. The selection of Al7075 is driven by its superior strength-to-weight ratio, coupled with exceptional fatigue resistance, fracture toughness, and compressive strength [31].

Table 1. Al7075 composition. Source: [31].

Composition	Al	Cu	Mg	Zn	Cr	Mn	Si	Fe	Ti
(wt %)	88.77	1.92	2.53	6.09	0.19	0.09	0.09	0.26	0.06

Table 2. Al7075 mechanical characteristics. Source: [32].

Mechanical Properties	**Value (GPa)**
Modulus of Elasticity	71.7
Ultimate Tensile Strength (UTS)	0.572
Tensile Yield Strength	0.503
Shear Strength	0.331
Modulus of shear	26.9

E. POWDER SELECTION

1. Aluminums 7075

As noted in the previous section, Al7075 offers numerous advantages. The critical velocity (V_{Cr}) for Al7075 was calculated using a simplified equation derived from "A Simplified Approach for the Determination of Critical Velocity for Cold Spray Processes," incorporating minimal parameters such as melting temperature (T_m), initial temperature (T_i) and specific heat capacity (C_p). The V_{Cr} from Equation (1) closely corresponds to a 40µm Al7075 particle, as shown in Figure 7. For Al7075 with values of Ti = 25 °C, T_m = 635 °C, and C_p = 0.96 J/g °C, the critical velocity is 630 m/s. This value is somewhat less than that reported in Figure 7. It is of note that the critical velocity was not sensitive to the particle size at least in the range reported.

$$V_{Cr} = \sqrt{Cp\ (\ 0.7\ T_m\ -\ T_i)} \tag{1}$$

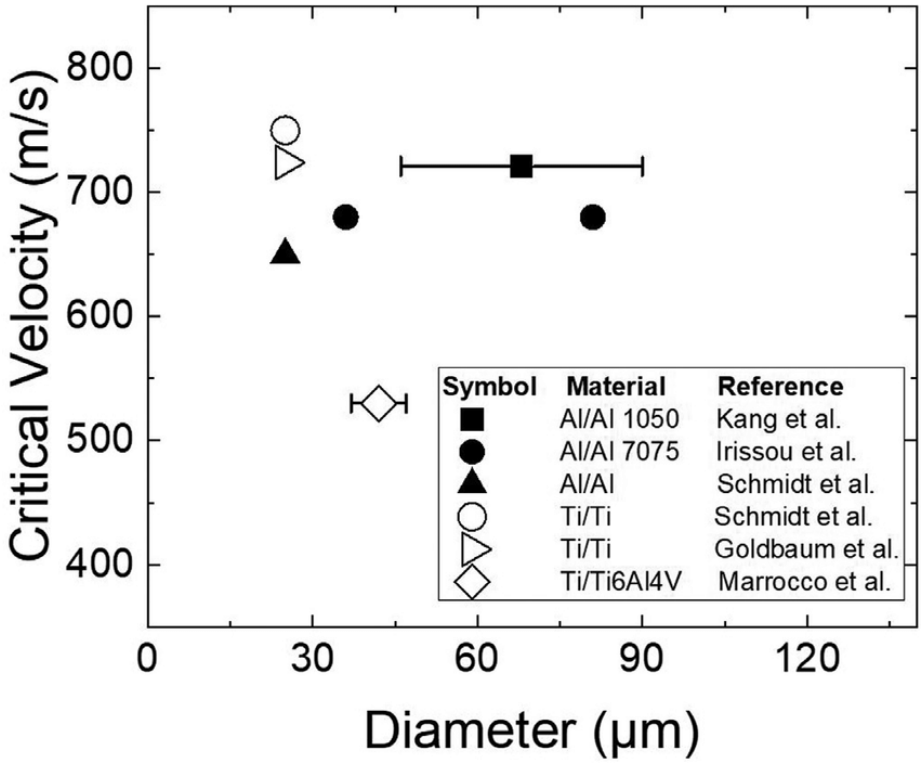

Figure 7. Critical velocities of various metals and alloys. Source: [33].

2. Boron Carbide

Boron carbide (B_4C) is among the most exceptionally hard synthetic materials, surpassed in hardness only by diamond and cubic boron nitride [34]. The unique properties of B_4C, such as its low density (2.52 g/cm³), superior hardness (Knoop 100 g), ranging from 2900 to 3580 kg/mm², and high melting point, making it an ideal choice as a reinforcement material for Al7075 [35]. This combination of attributes provides B_4C with outstanding wear and thermal resistance, which renders it invaluable in applications involving cutting tools and armor [35]. The ability to withstand high temperatures and resist wear is a key factor contributing to its frequent use in these fields.

Another noteworthy aspect of B_4C is its remarkable neutron absorption capacity, primarily owing to the presence of the naturally occurring B-10 isotope. This isotope is particularly efficient at absorbing neutrons and constitutes approximately 20% of boron atoms [34]. This neutron-absorbing capability makes B_4C an important material in nuclear and radiation shielding applications, where its ability to capture neutrons plays a role in

enhancing safety and radiation containment. Boron carbide with its features such as hardness, low density, high melting point, and exceptional neutron absorption capacity, is a versatile material with a wide range of practical applications, from cutting tools to nuclear safety measures.

3. Boron Nitride Nanotubes

As highlighted in the "Recent advances and perspective on boron nitride nanotubes: From synthesis to applications," boron nitride nanotubes (BNNT) have emerged as a noteworthy class of nanomaterials. They share structural similarities to that of carbon nanotubes (CNT) as seen in Figure 8. The distinct chemistry, however, of BNNT leads to different properties when compared to CNT. These nanotubes exhibit elevated thermal stability compared to CNT, are electrical insulators (CNT are an electrical conductor), exhibits optical transparency, high neutron absorption, and displays piezoelectric behavior [36]. Moreover, BNNT, containing boron and nitrogen, possess larger neutron capture cross-sections [37]. This means enhanced radiation shielding capability in BNNT [38]. This is why boron nitride is used for radiation shielding in nuclear reactors and why BNNT may excel as radiation shielding in spacecraft.

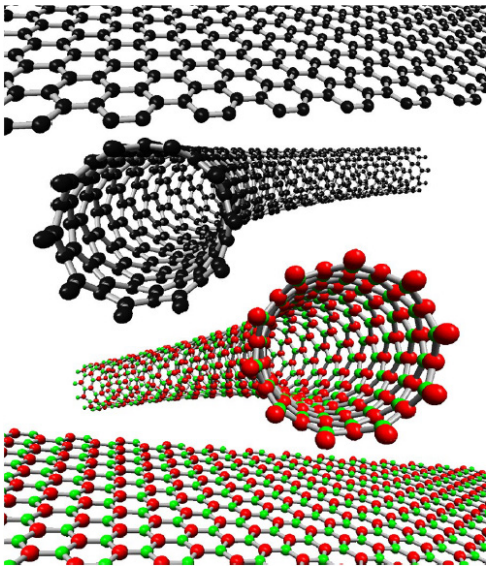

Figure 8. Ball-stick structural model of graphene sheet and single-wall CNT (top) along with h-BN sheet and BNNT (bottom). The black atoms represent carbon, red atoms represent boron, and the green atoms represent nitrogen. Source: [36].

F. FUNCTIONALLY GRADED COATINGS

Functionally graded coatings (FGC) are a class of engineered surface treatments that exhibit a gradual transition in composition, leading to a transition of material properties. The coating is transiting from one material and/or phase to another. These coatings have garnered substantial interest due to their ability to provide multifunctionality and tailored properties, such as enhanced wear resistance, corrosion protection, and thermal insulation. A simple example of a functionally graded coating is that often used in gas turbine engines. Figure 9 shows an example schematic of the multiple layers, including the thermal barrier coating (TBC), that would be deposited over a Ni superalloy (metal substrate). A TBC is a low-thermal conductivity refactory ceramic used to insulate the metallic components [39]. The problem is differences in thermal expansion between the metallic substrate and the TBC necessitates intermediate layers. Delamination or layer fretting is often an issue with these coatings when the layers are distinct. Depositing the layers such that the interfaces are compositional gradients may mitigate problems that arise when the layers are distinct.

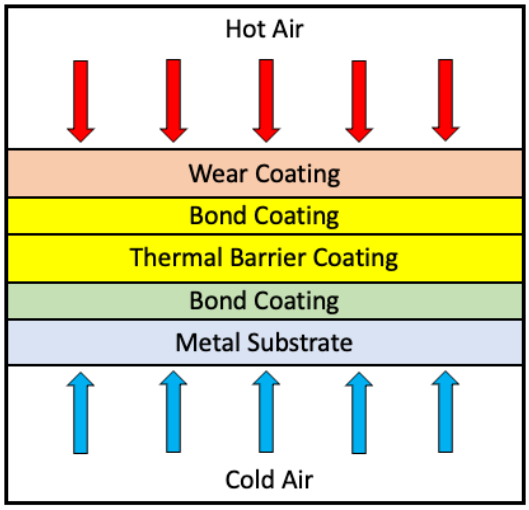

Figure 9. Multi-layer coating schematic.

FCG serve to tailor properties best suited to the specific environment encountered. For example, the integration of fine B_4C particles into Al-alloy material could bolster pitting corrosion resistance, while keeping the ductility of Al and leading to an increase in coating hardness. benefit that becomes more pronounced with higher B_4C particle weight percentages. However, this enhancement in pitting corrosion resistance may come with an elevated risk of grain boundary segregation, owing to the finer size of the reinforcement [40]. A schematic of the various dimensional composite reinforcements found in MMC is shown in Figure 10. For this work, the Al7075 is reinforced with particles (i.e., B_4C) and/ or short fibers (i.e., BNNT).

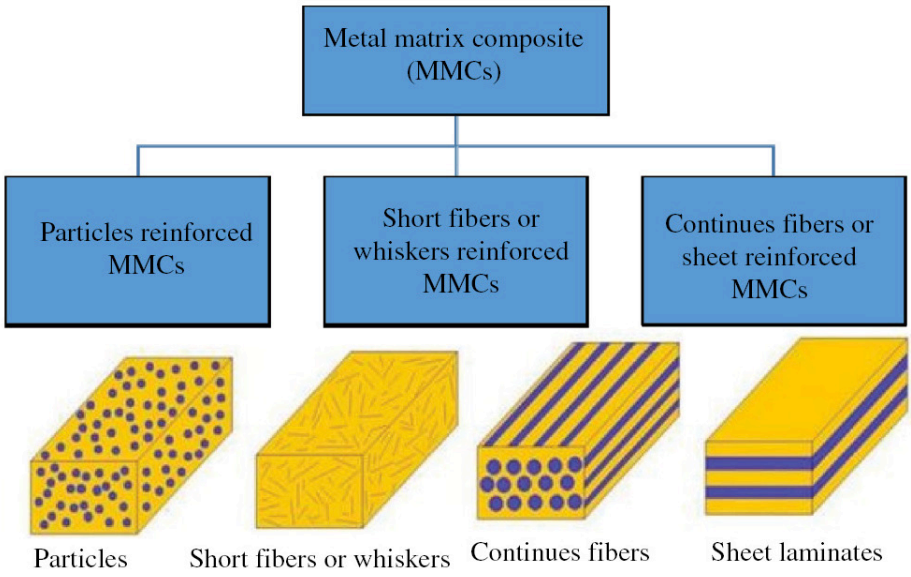

Figure 10. Metal matrix composite reinforcer phases. Source: [41].

The friction coefficient between the MMC and the base matrix material is another factor that significantly influences wear rates. Low friction coefficients have the advantage of reducing abrasive wear, as well as diminishing heat generation, ultimately leading to lower wear rates [42]. These factors collectively make MMCs with ceramic reinforcers an enticing prospect for a range of industrial applications, especially when durability and wear resistance are paramount [29].

G. POWDER PROCESSING

The quality of the powder feedstock plays a pivotal role in the success of cold spray deposition, directly influencing crucial coating properties like adhesion, density, and mechanical performance. Cold spray powders are typically characterized by their fine-grained nature and a narrow size distribution. They should exhibit high levels of purity with minimal impurities. Additionally, the morphology of the powder particles, including their shape and size, can significantly affect both the deposition process and the resulting coating quality. It is essential that the powders are free-flowing and free from agglomerates or moisture. Various methods can be employed to create powders suitable for cold spray applications, such as gas atomization, mechanical milling, and gas condensation.

High-energy ball milling (HEBM) is a mechanical processing technique that involves the use of a ball mill to crush, blend, or grind materials into extremely fine powder particles. The term "high-energy" refers to the significant kinetic energy that is imparted to the milling balls and the materials being processed during the milling process. This high kinetic energy results from the rapid rotation and motion of the milling balls within a milling chamber or vessel. The ball-to-powder ratio (BPR) and the milling time have been shown to have a significant impact on the properties of the particles (see Figure 11) in the HEBM process [43]. Other factors that can influence the effectiveness of HEBM is the milling speed, temperature control to prevent unwanted thermal reactions, and milling atmosphere.

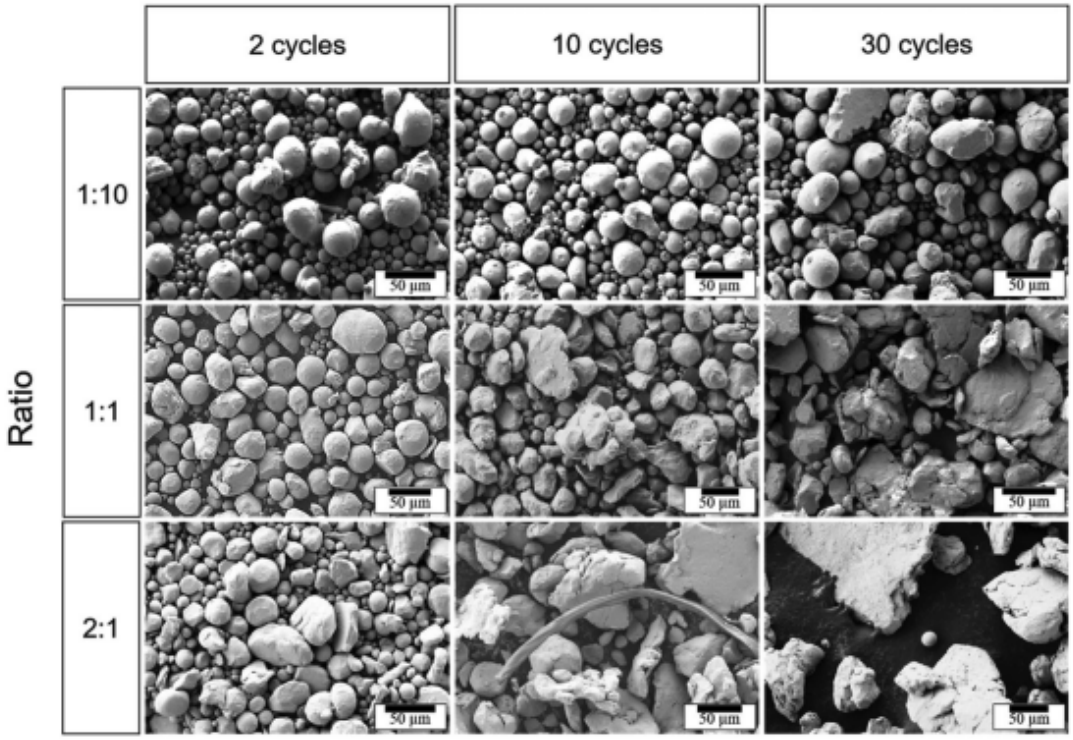

Figure 11. SEM images of milled 316L stainless steel powders processed at different BPRs and under varying cycles. Source: [44].

THIS PAGE INTENTIONALLY LEFT BLANK

III. MATERIALS AND EXPERIMENTAL PROCEDURES

A. MATERIAL SELECTION

In this study, Al7075 was selected as the substrate material due to its properties, particularly its relatively high fatigue resistance and other advantages discussed in the previous chapter. Enhancing the Al7075 foundational material in cold spray applications can be achieved by incorporating ceramic materials as reinforcements within the matrix. The Al7075 powder utilized in this experiment was sourced from Solvus Global in Worcester, MA (SAAM-AL7075-G1H1). The composition of the powders used in this study is shown in Table 3. The original state of the Al7075 particles from the manufacturer revealed a spherical morphology with three distinct diameters, ranging from 18μm to 51μm, as illustrated in Figure 12. While the high-energy ball milling (HEBM) process may affect the powder's shape and overall morphology, the primary objective remains the preservation of Al-7075's spherical shape.

Table 3. Solvus powder composition. Source: [45].

Composition	Al	Cu	Mg	Zn	Cr
(wt %)	Balance	0.18 – 0.28	2.1 – 2.9	5.1 – 5.6	0.18 – 0.28

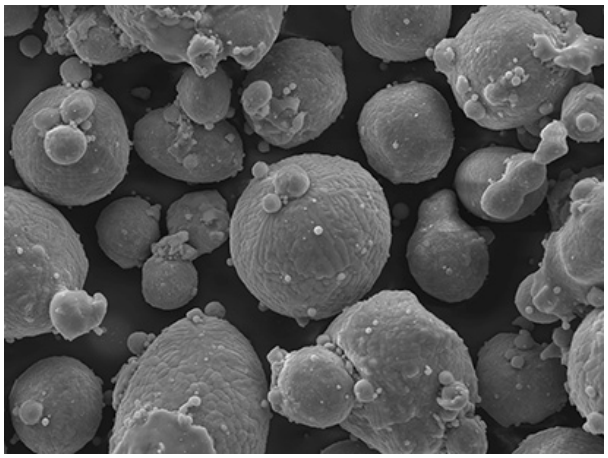

Figure 12. TEM image of SAAM-AL7075-G1H1 powder. Source: [45].

Two distinct types of B_4C powder were employed, both sourced from U.S. Research Nanomaterials Inc. in Houston, TX. The first type, μB_4C (12069-32-8), with a diameter ranging from 1 to 3μm as depicted in Figure 13, was utilized in the initial three layers of the functional graded coating. The second type, nB_4C (12069-32-8) as seen in Figure 14, was used in the final top layer.

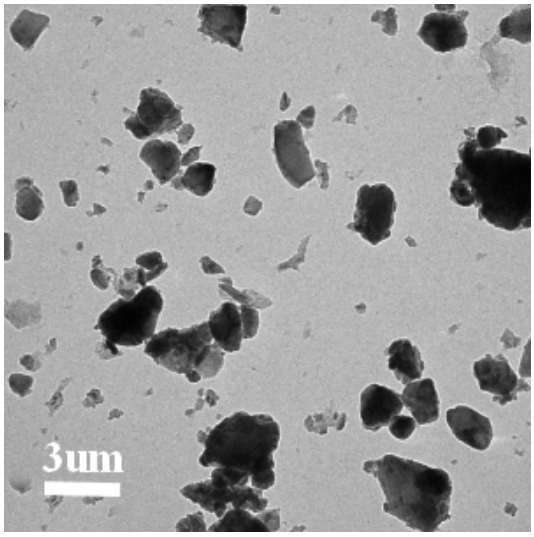

Figure 13. TEM image of μB_4C powder. Source: [46].

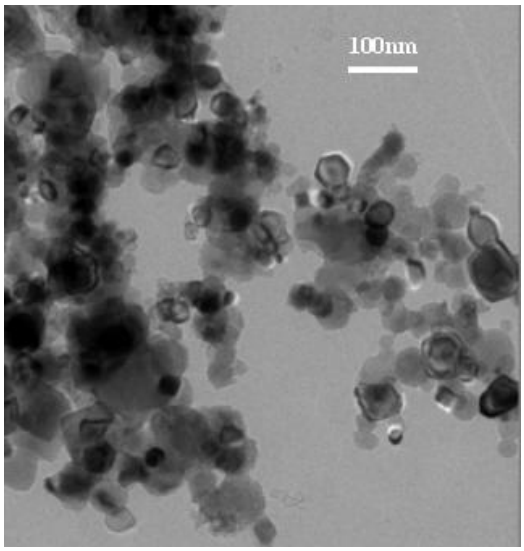

Figure 14. TEM image of nB4C powder. Source: [47].

The BNNT used in this study were from BNNano Inc. (Burlington, NC, USA). which is referred to as "NanoBarbs" (BNNB-P-90A1) from the manufacturer. This unique feature of the nanobarb is that it has irregularities along the nanotubes which act like mechanical "barb" to assist with interlocking to matrix materials [48]. A TEM image of a nanobarb BNNT can be seen in Figure 15. All of the materials used in this thesis is listed in Table 4.

Figure 15. TEM image of a BNNT, as received from manufacturer. Source: [49].

Table 4. Material Parameters and Identification.

Material	Composition	Powder Size	Vendor	Identification
Aluminum	Al-7075	Diameters (various mix) 18 ± 10% µm 33 ± 10% µm 51 ± 10% µm	Solvus Global	SAAM-AL7075-G1H1 Type 1–01
Boron Carbide	nB_4C	Diameter: 45–55nm	US Research Nanomaterials Inc.	12069-32-8
Boron Carbide	µB_4C	Diameter: 1–3µm	US Research Nanomaterials Inc.	12069-32-8
Boron Nitride Nanotubes	BNNT	Width: 60 nm Length: 20 µm	BNNano Inc.	BNNB-P-90A1

B. HIGH ENERGY BALL MILLING

Four compositions were milled together for the final functionally graded coating, following the volume percentages outlined in Table 5. The concentration of µB_4C increased with each subsequent layer, except for the final one. As the vol.% of µB_4C increases, the

DE decreases resulting in thinner layers. This layering process increased the thickness of the applied LPCS to protect the substrate from wear during testing.

Table 5. Functional graded coating composition summary.

Layer	Al [vol.%]	μB_4C [vol.%]	nB_4C [vol.%]	BNNT [vol.%]
1	90	10	0	0
2	85	15	0	0
3	80	20	0	0
4	96	0	2	2

For each composition to be cold sprayed, 200 grams of powder was created. The densities of each material used is listed in Table 6. The densities were needed to accurately determine the amount of powder placed in the milling canisters. Each composition required four batches of 50 grams to be done at a time due to the size of the holding stainless steel canisters required for mixing. A BPR (ball to powder ratio) of 1:5 was utilized for each sample consisting of 10 grams of 302 stainless steel balls. A pattern of mixing for five minutes followed by a five-minute settling time was utilized when mixing the compositions. This was done to allow the samples to cool down between ten cycles. The parameters used during HEBM are listed in Table 7.

Table 6. Powder densities.

Powder	Density [g/cm^3]
Al	2.70
B_4C	2.52
BNNT	2.1

Table 7. HEBM parameters for all MMC compositions.

Mass of Powder	Milling Media	Containment	BPR	Interval	Cycles
50g	3mm 504 SS Balls	SS Canister	1:5	5 min on / 5 min off	10

SPEX SamplePrep Mixer/Mill 8000D, seen in Figure 16, was the milling machine used to mix the compositions. This machine operates 1060 cycles per minute. The BPR of 1:5 was based on a study conducted by Samuel Rice that with this ratio and pattern of 5 minutes on followed by 5 minutes off for 10 cycles created a uniform powder distribution while retaining the powders original morphology [5].

Figure 16. SPEX SamplePrep Mixer/Mill 8000D.

When mixing the powders, adequate space was provided which was different from that of a previous study conducted by David Tauber [49]. 50-gram batches were utilized vice 60-gram batches that was used to allow additional space in the containment cylinder to allow the stainless-steel balls to achieve a higher velocity to impact the powders when

mixing. This also eliminated the need for packing the powders initially when filling the canisters as compared to 60-gram batches.

C. COLD SPRAYING AND STORAGE

After the composite powders were created from the HEBM process, the powders were transferred to glassware. From there, the powders were placed in a vacuum oven at 90 °C for a minimum of 24 hours at a vacuum of ~ 0.9 bar to remove any moisture. A low pressure cold (LPCS) system was utilized using a Centerline Supersonic Spray Technologies division (SST) Series P Spray Machine with an Automatic Spray Gun and an added X-Feeder, seen in Figure 17.

Before spraying any samples were conducted, it was noted that the powder feed line was consistently clogging with higher concentrations of μB_4C. When any vol%. of BNNT was used in the spray process, there were no issues with clogging of the powder feed line noted. The line was replaced prior to testing and the nozzle assembly properly blown out with compressed air which alleviated any complications during cold spray process.

Figure 17. Centerline SST system.

Individual samples were tested using a single pass of different Al7075 MMC compositions with μB_4C prior to attempting a functionally graded coating. This was done to determine the upper limit of the volume percentage of μB_4C before deposition onto the substrate showed a significant decrease. Additional Al7075 MMC compositions were attempted utilizing nB_4C and BNNT to see if any added benefits could be gained from first spraying these directly onto an Al7075 substrate.

Table 8. Individual test samples.

Sample	Al [vol.%]	μB_4C [vol.%]	nB_4C [vol.%]	BNNT [vol.%]
1	90	10	0	0
2	80	20	0	0
3	70	30	0	0
4	96	0	2	2
5	94	0	5	1
6	100	0	0	0

Initially, N_2 was used as the carrier gas. The parameters that eventually led to some deposition of the Al7075 Solvus powder while testing the powder feed line can be seen in Table 9.

Table 9. N_2 spraying parameters.

Nozzle Temperature	Gas Pressure	Standoff Distance	Feed Rate	Traverse Speed	Line Spacing
550°C	1.52 Mpa	12.7 mm	9.7 g/min	20 mm/s	1 mm

Later, He was chosen as the carrier gas as it has been shown to be a more effective carrier gas with better deposition [22], [23]. Individual Al7075 substrates were sprayed with a single pass coating to determine a general coating thickness for each pass using the following parameters. To clarify, a single pass coating is to only apply one application of a particular powder. In a double pass coating, a layer that was just applied would be resprayed with that same powder. In both He and N_2 multiple spray parameters such as spray temperature, pressure, standoff distance, feed rate, and standoff distance were adjusted. The parameters given yielded the best results with given configuration of the Centerline SST assembly are listed in Table 10. Furthermore, it was at the upper end limits of what the heater could maintain with the respective carrier gases when spraying.

Table 10. He spray parameters.

Nozzle Temperature	Gas Pressure	Standoff Distance	Feed Rate	Traverse Speed	Line Spacing
310°C	1.15 Mpa	12.7 mm	9.7 g/min	10 mm/s	1 mm

D. METALLURGICAL PREPARATION

1. Cutting

After samples were cold sprayed, they were cut into smaller sections for microstructural analysis. These samples were cold mounted and polished using a Struers cutting machine at 3000 RPM using a 1.0 mm/s advance speed (Figure 18).

Figure 18. Struers Secotom-20 cutting machine.

2. Cold Mounting

Cold mounting was performed using a two-part epoxy resin from Allied High Tech Products Inc. Both the epoxy and hardener had to be mixed per the manufacturer's recommendations. Once the sample was cut, it was placed in the silicon mold, covered in epoxy, and allowed to cure for approximately 24 hours. The cured epoxy formed a puck that was then able to be mounted for polishing. This process was used primarily for cut samples, but a few powder samples were cold mounted by placing a thin layer of powder at the bottom of the silicon mold before pouring in the epoxy.

3. Polishing

Prior to placing samples under the optical microscope, the following parameters were utilized in polishing samples in Table 11. A Buehler Ecomat 4 Automatic Polisher was primarily used throughout the process, but the final steps resulted in excessive scratches in the samples.

Table 11. Polishing parameters.

Step No.	Grit/Solution	Time	RPM	Force (lbs)
1	320	5 min	250	5
2	500	10 min	250	5
3	800	15 min	250	5
4	1200	15 min	250	5
5	1 μm Alumina	10 min	250	Hand polish

An attempt to use 1 μm alumina on a polishing cloth was attempted which resulted in discoloration and pitting of the sample when placed under the automatic polisher for 30 minutes at 250 RPM. This can be attributed to the higher concentrations of B_4C in the samples conducted and was more than likely the result of the B_4C becoming dislodged from the sprayed coating and embedding itself into the substrate. To remedy this, the samples were each hand polished with 1 μm alumina for approximately 10 minutes until the samples had a mirror like finish and reduced scratching could be seen under the optical microscope. The samples were then chemically etched using a Keller's reagent to expose the grain boundaries and microstructure when placed under a microscope.

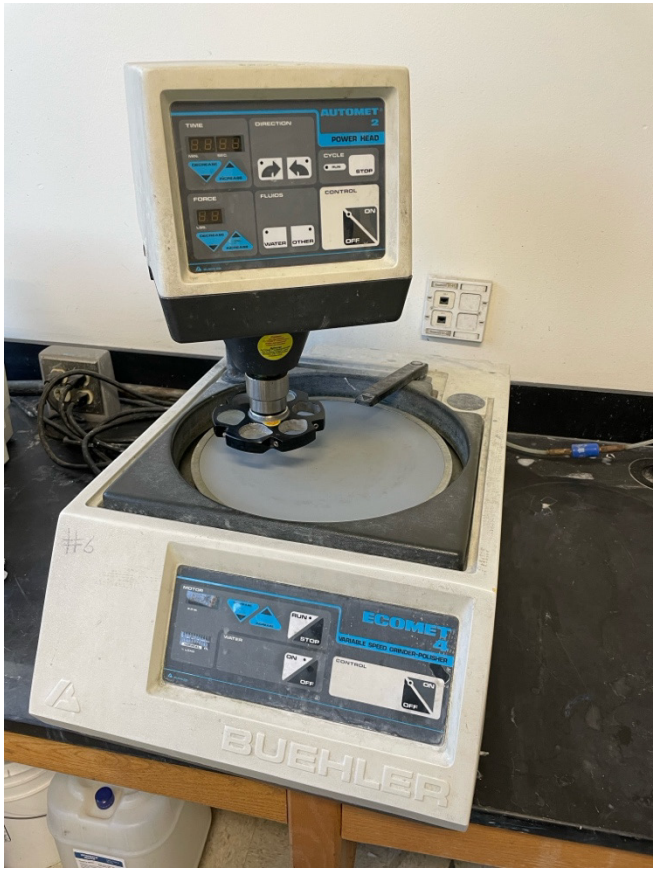

Figure 19. Buehler Ecomet 4 automatic polisher.

E. MECHANICAL WEAR TESTING

To assess the coating's resistance to degradation over time, wear testing was carried out. Given the graded nature of the coatings, initial susceptibility to wear primarily pertained to the topcoat. For evaluation, the top-coats consisting of 2% BNNT and 2% nB_4C were compared to a 20% μB_4C layer as well as a sample of sprayed Al-7075.

Wear resistance tests involved a series of three dry sliding wear tests at different loadings utilizing a ball-on-disk configuration. Samples featured a topcoat comprising of multiple layers of cold spray coating, ensuring an adequate coating depth for the test's duration. These wear tests as seen in Table 12 focused on evaluating the surface of the coating, rather than assessing the cross-section.

Table 12. Wear testing parameters.

Test	Applied Load (N)	RPM	Test Duration (min)	Wear Track Diameter (mm)	Total Sliding Distance (m)	Counter Surface
Ball-on-Disk	1	100	60	3	56.5	3 mm SS 304 ball
Ball-on-Disk	3	100	60	3	56.5	Ball-on-Disk
Ball-on-Disk	5	100	60	3	56.5	Ball-on-Disk

The wear tests were executed using a Nanovea T50 modular tribometer, as depicted in Figure 20. Prior to performing the wear tests, each sample was sectioned from a larger piece employing a Struers Secotom-20 high-speed saw, as previously illustrated in Figure 18, facilitating placement in the tribometer. Mass measurements were taken before and after each test to calculate mass loss. A 3 mm stainless steel 304 ball was used as the wearing surface. A new stainless-steel ball was installed for each individual test.

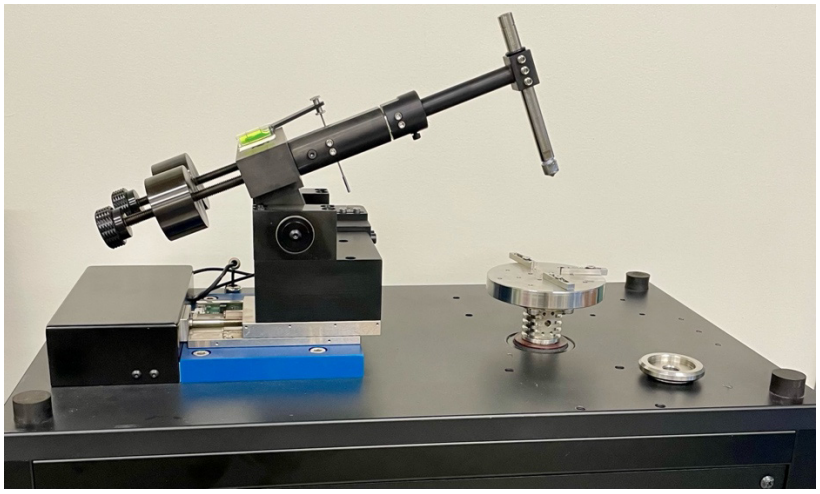

Figure 20. Nanovea T50 modular tribometer.

Throughout the test, the tribometer's encoder measured wear depth and continuously recorded the coefficient of friction. Data collection occurred at a rate of 20 data points per second. The applied load for the tests was set at 1N, 3N, and 5N, and the wear tracks had a diameter of 3 mm. The sample rotated at 100 RPM for a duration of 1 hour, resulting in a total sliding distance of 56.5 meters.

F. CHARACTERIZATION

Microscopic examination was conducted on both powdered and sprayed samples. The powdered samples were affixed to SEM sample stubs using double-sided carbon tape and then stored appropriately in a vacuum chamber before SEM inspection was conducted. Before undergoing analysis in the SEM, all the mounted samples were first inspected using a Nikon Model Epiphot 200 Microscope equipped with a Nikon Digital Sight DS-2Mv. The Nikon microscope's lower magnification, which spans from 2.5 to 100 times in both light and dark fields, was employed for the visual examination of the samples prior to their transfer to the SEM for more comprehensive analysis. The SEM used is this study was a Helios 5 UX SEM seen in Figure 21. Various parameters were utilized during SEM operations based on the sample and composition being analyzed.

Figure 21. Helios 5 UX SEM.

THIS PAGE INTENTIONALLY LEFT BLANK

IV. RESULTS AND DISCUSSION

A. POWDER COMPOSITION AND CHARACTERIZATION

The SEM was utilized to capture images of all powder compositions post HEBM to confirm the preservation of the base powder's spherical morphology and the even distribution of ceramic reinforcements. The initial imaging of Al7075 powder, obtained from the manufacturer, was conducted prior to HEBM processing. Figure 22 illustrates the powder's spherical morphology, featuring distinct sizes ranging from approximately 18 to 51 µm.

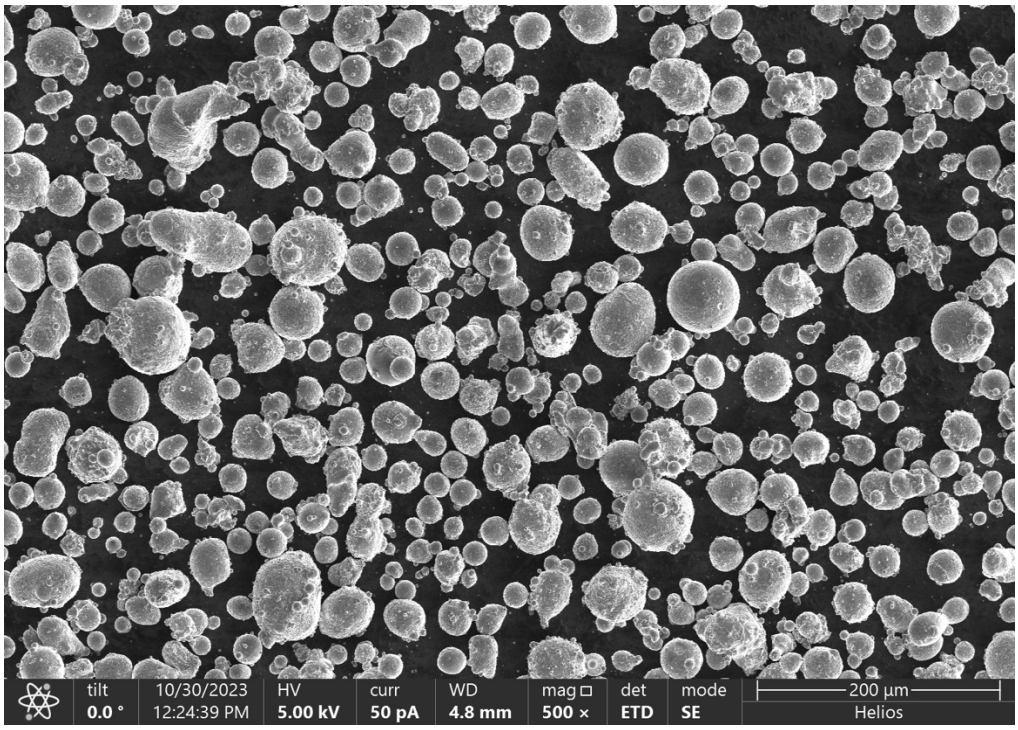

Figure 22. SEM solvus powder.

1. Al7075 and µB$_4$C

The Al7075 powder received from the manufacturer was mixed with various vol.% µB4C. A mixture of 30% µB4C was successfully sprayed in trial runs but it was noted that as the vol.% µB4C increases, the lower the DE efficiency was obtained. For this reason, a

15% µB4C composite powder was created and applied to the FGC. Also, 30% µB4C as a layer was omitted from the final FGC.

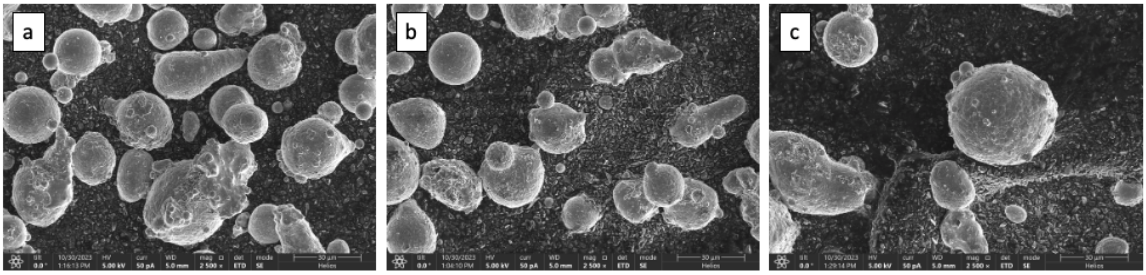

Figure 23. Powder disbursement for a) 10 vol.%, b) 15 vol.%, and c) 20 vol.%.

SEM images of all three µB_4C composite powders are seen in Figure 23. The larger, spherical particles are the Al particles. Dispersed in between the Al particles are the smaller µB_4C platelets. In Figure 24, a closeup of the 30% powder is seen where µB_4C particles are both adhering and not-adhering to an Al particle.

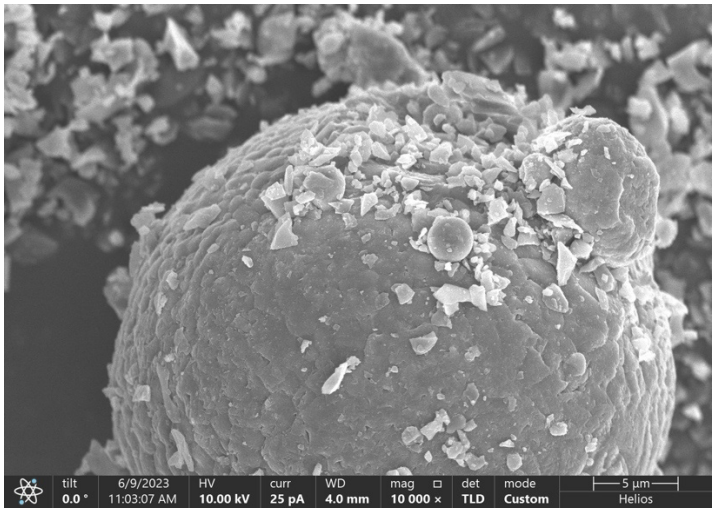

Figure 24. Powder disbursement for 30 vol.%.

2. Al7075, nB$_4$C, and BNNT

The same Al7075 powder was milled with 2% nB$_4$C and 2% BNNT for the dual reinforced top-layer. The milled powders are seen in Figure 25. It was observed that during the HEBM process, when sifting powders to remove the stainless-steel balls, those containing BNNT exhibited smoother flow compared to both the base Al7075 powder and those with µB$_4$C. It should be noted, however, that rheology measurement was not performed and so this is a qualitative observation. Higher vol.% µB$_4$C compositions showed an increased tendency toward powder clumping, particularly notable in the 30 vol.% µB$_4$C. This observed increase in clumping may mean increased particle agglomeration, potentially contributing to lower deposition rates of the µB$_4$C composite powders. This observation extended to the cleaning process of the powder feed line and container post-cold spray application. A higher vol.% µB$_4$C MMC would often clog the powder feed line during the cold spray process. This was not the case when BNNT was incorporated into the MMC. Furthermore, use of BNNT would exhibit a more favorable cleaning behavior when removing the material from the powder canisters post spray and not leave clumps attached to the auger compared to a µB$_4$C MMC.

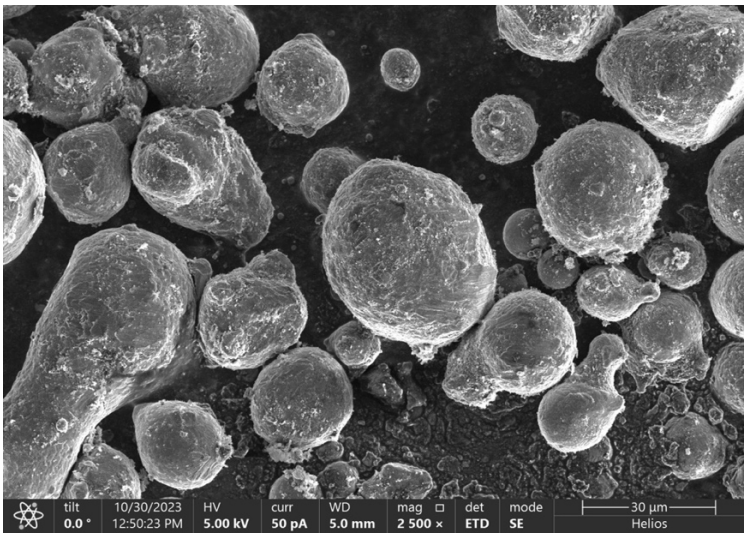

Figure 25. 2 vol.% nB$_4$C with 2 vol.% BNNT.

B. COLD SPRAY SAMPLE CHARACTERIZATION

1. Visual Inspection

Following cold spray , a comprehensive visual inspection was performed, concentrating on evaluating uniformity, porosity, and thickness. The FGC was sprayed with offset passes, as depicted in Figure 26, enabling surface analysis of different compositions and their wear properties. To note, all layers were sprayed with a single pass, except for one sample. This particular sample had two passes sprayed but only of the top layer, composed of 2 vol.% nB4C and 2 vol.% BNNT. All other layers of this sample were sprayed as a single pass. This sample is referred to as the dual pass sample going forward.

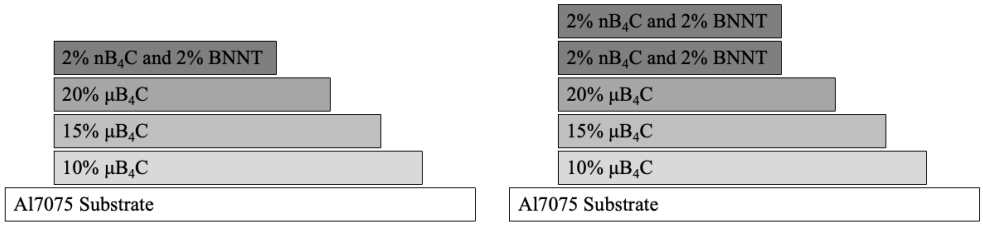

Figure 26. Single pass 2% nB4C and 2% BNNT FGC with offset (left) and dual pass 2% nB4C and 2% BNNT FGC with offset (right).

In Figure 27 and Figure 28, layered functionally graded coatings are seen after spraying. Notably, coatings with a higher vol.% µB4C exhibited a slightly darker contrast than its preceding layer. All coatings exhibited even distribution, without any raised edges or nonuniform coating thickness, commonly associated with the path of the deposition nozzle during application. There was no discernible visual variation in porosity among the coatings post-spraying.

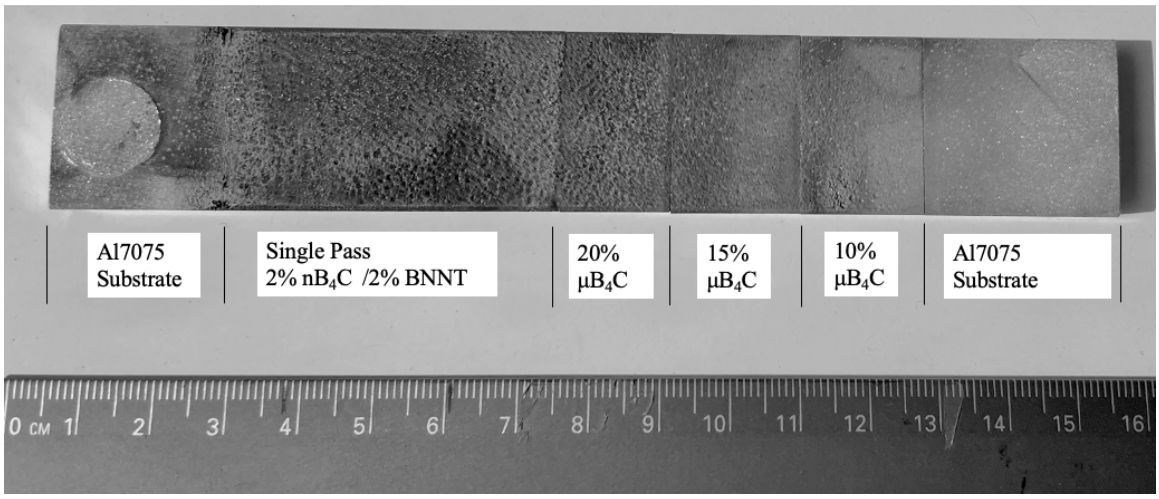

Figure 27. Single pass 2% nB_4C and 2% BNNT FGC.

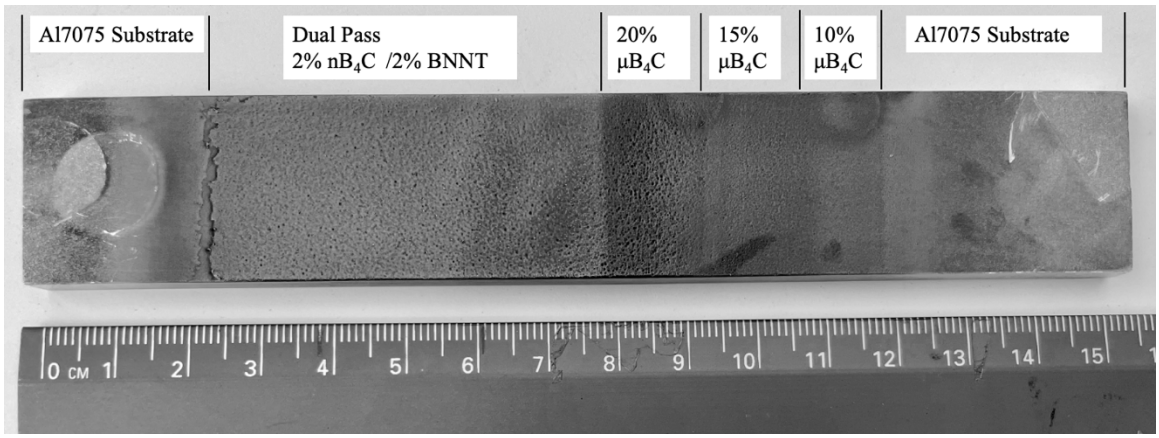

Figure 28. Dual pass 2% nB_4C and 2% BNNT FGC.

There was a noticeable distinction between the coatings applied with a single pass of 2% nB_4C and 2% BNNT compared to those with a dual pass. The sample subjected to the dual pass exhibited a smoother finish, both to the touch and to wear testing, in contrast to the single pass sample.

2. Optical Microscopy

All samples underwent optical microscopy analysis (some of these optical images are seen in Figure 29), where live images were captured using the optical microscope detailed in Chapter III. These images served to assess the efficacy of cold spray deposition

between samples and to verify the quality of polishing on cross-sectioned samples before subjecting them to chemical etching or SEM analysis. This process aimed to minimize visible surface scratches, ensuring accurate characterization both the optical microscope and in the SEM.

Figure 29. Optical microscope images of three compositions. Starting left to right: 10 vol.% μB_4C with Al7075, 20 vol.% μB_4C with Al7075, 30 vol.% μB_4C with Al7075.

Table 13. Layer thickness of compositions.

Sample	High (μm)	Low (μm)	Average (μm)
10 vol.% μB_4C	671.43	542.86	607.14
20 vol.% μB_4C	578.57	425.08	501.83
30 vol.% μB_4C	285.71	175.03	230.37

The samples in Figure 29 illustrate a significant decrease in DE with the application of higher volume percentages of μB_4C. The drop became noticeable at 30 vol.% μB_4C, as shown in Table 13 prompting the decision to limit the application to a maximum of 20 vol.% μB_4C when employing the FGC. This limitation was likely attributed to the increased concentration and hardness of B_4C, preventing plastic deformation upon impact during cold spraying. Additionally, higher volume percentages of μB_4C were observed to cause more frequent clogging of the powder feed line. The parameters utilized for the three samples in Figure 29 remained constant during the cold spray process.

Additional samples were tested, consisting of nB_4C and BNNT compositions. In Figure 30, it is evident that minimal depositions were achieved when these samples were directly sprayed onto the Al7075 substrate. The micron-thick layers were scarcely discernible upon visual inspection but in cross-sectional images taken under the optical microscope were observed. The composition of 2 vol.% nB_4C and 2 vol.% BNNT did appear to have more material deposited onto the substrate as compared to other composite coatings, specifically 5 vol% nB_4C/1 vol.% BNNT.

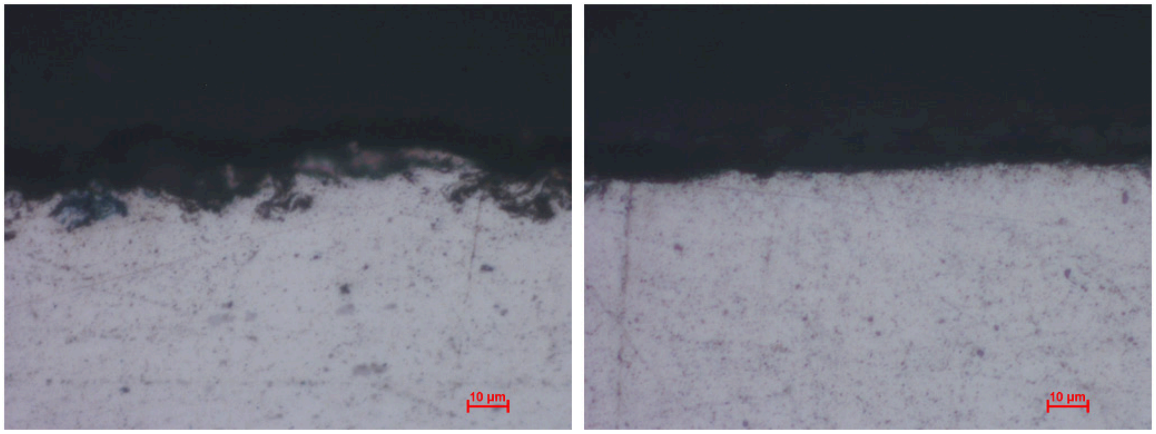

Figure 30. Optical microscope of two compositions. The 2vol.% nB_4C/2% BNNT with Al7075 (left) and 5 vol.% nB_4C/1 vol.% BNNT with Al7075 (right).

3. SEM Microstructural Characterization

The gradients between layers were observed in the single-pass FGC. The transition between vol.% μB_4C layers is visible at lower magnification, an example is seen in Figure 31. Similar to the 2 vol.% nB_4C and 2 vol.% BNNT layer discussed earlier, it exhibited lower deposition compared to the layers containing μB_4C and could not be easily identified at lower magnification.

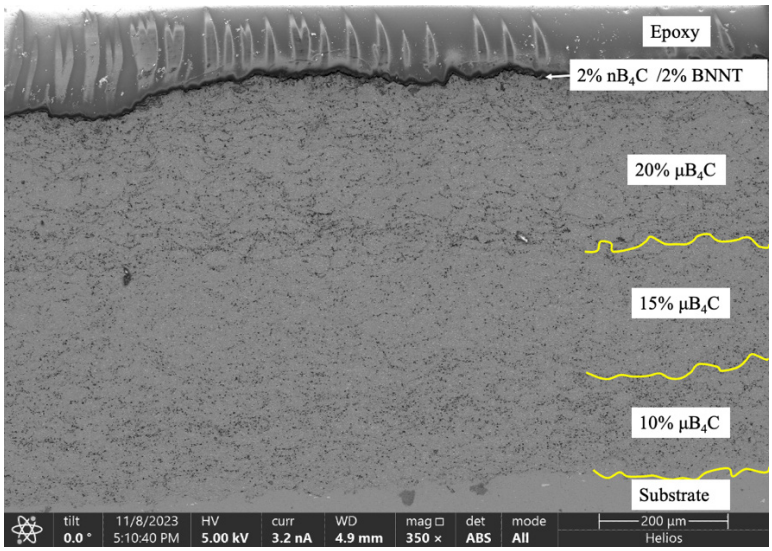

Figure 31. SEM single pass FGC cross section.

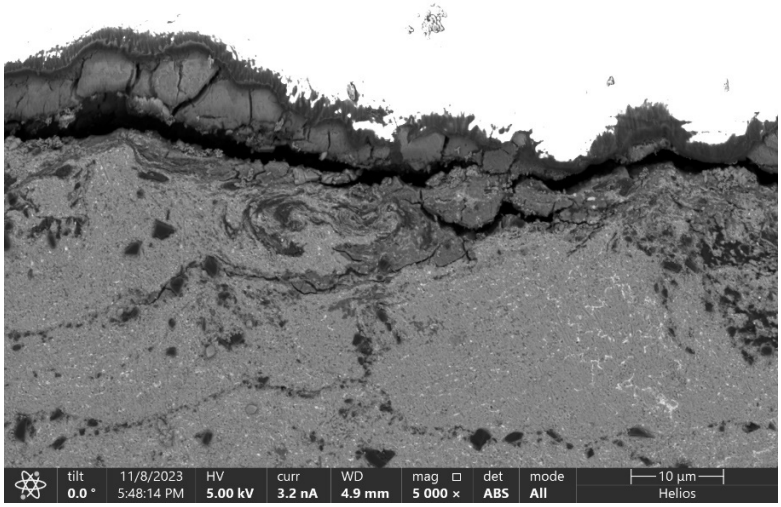

Figure 32. SEM single pass cracking of the 2 vol.% nB4C / 2 vol.% BNNT layer.

When going to a higher magnification of the FGC, cracking is seen in the top layer where it meets the epoxy. The 2 vol.% nB4C / 2 vol.% BNNT layer also appears to be separating from the 20 vol.% µB4C layer below which is different in grain structure. This separation was continuous across the entire sample of the FGC and is a good indicator of poor adhesion taking place with this layer.

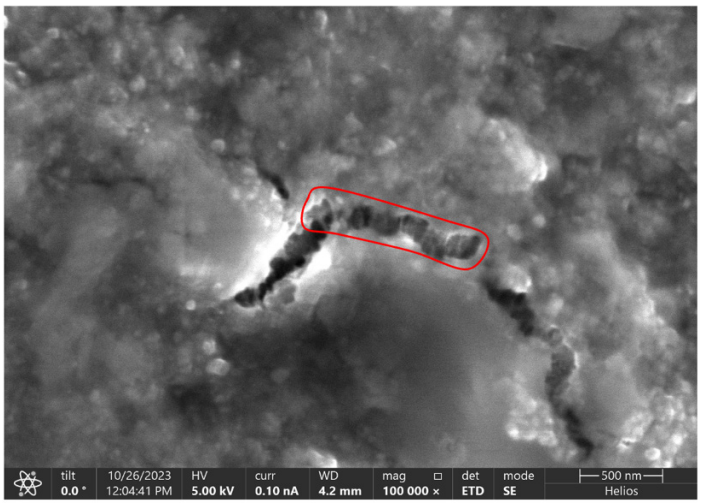

Figure 33. SEM top-down image of individual BNNTs located in Al/BNNT composition crater.

The incorporation of BNNTs and the low deposition rate is similar to the findings of another study by David Tauber [49]. The main difference with this layer was the use of nB$_4$C and BNNT. What appears to be BNNT is highlighted in red in Figure 33 can be seen in the crevice formed on the top layer. An attempt to confirm its elemental makeup through EDS was attempted, but due to its small size, was unable to get an accurate reading of the particles.

The FGC shown in Figure 34 was sprayed several days after the single pass coating. Its deposition was significantly less than that of the first coating that was cold sprayed initially. All the spray conditions were the same but along with the thickness being considerably less, the gradients between layers were not noticeable. Compared to the single pass coating, these powders were several days old but still maintained in a vacuum oven when not in use. The potential for powder contamination being an attributing factor is possible given that there were only two powder bins in the LPCS system utilized. This required powders to be changed out frequently.

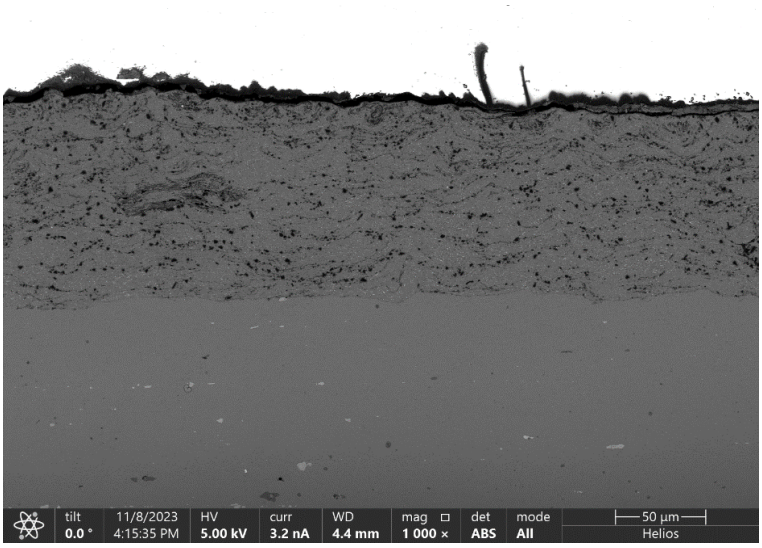

Figure 34. SEM dual pass FGC cross section.

The dual pass layer had the same characteristics of cracking in the 2 vol.% nB4C / 2 vol.% BNNT layer shown in Figure 35 and Figure 36 as with the first sprayed FGC. This further exhibits the poor adhesion characteristics of this applied powder. Evidence of any splat like formation common in the other layers with µB4C cannot be seen in this top layer.

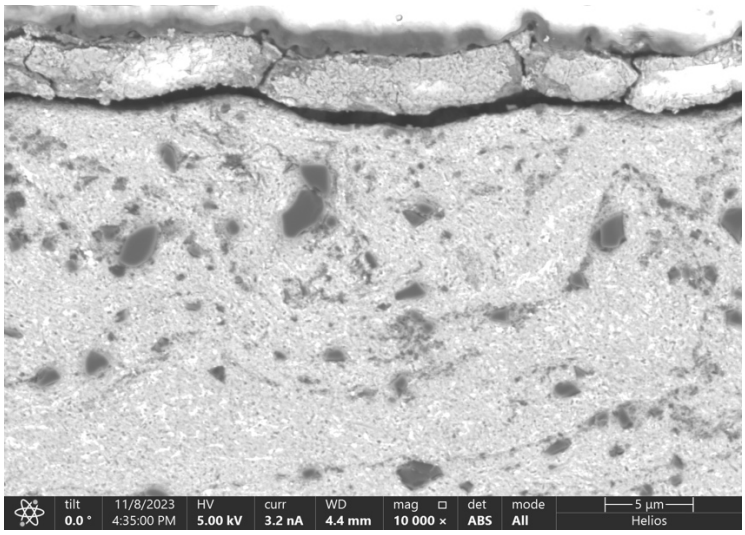

Figure 35. SEM dual pass cracking of the 2 vol.% nB4C / 2 vol.% BNNT.

Figure 36. SEM top-down image of dual pass 2 vol% nB4C / 2 vol.% BNNT.

The images seen in Figure 37 shows a top-down view of each individual composition taken in the SEM. There are subtle variations with each layer, but the dual pass coating significantly reduces the coarse structure found in 20 vol.% µB4C despite the coating thickness.

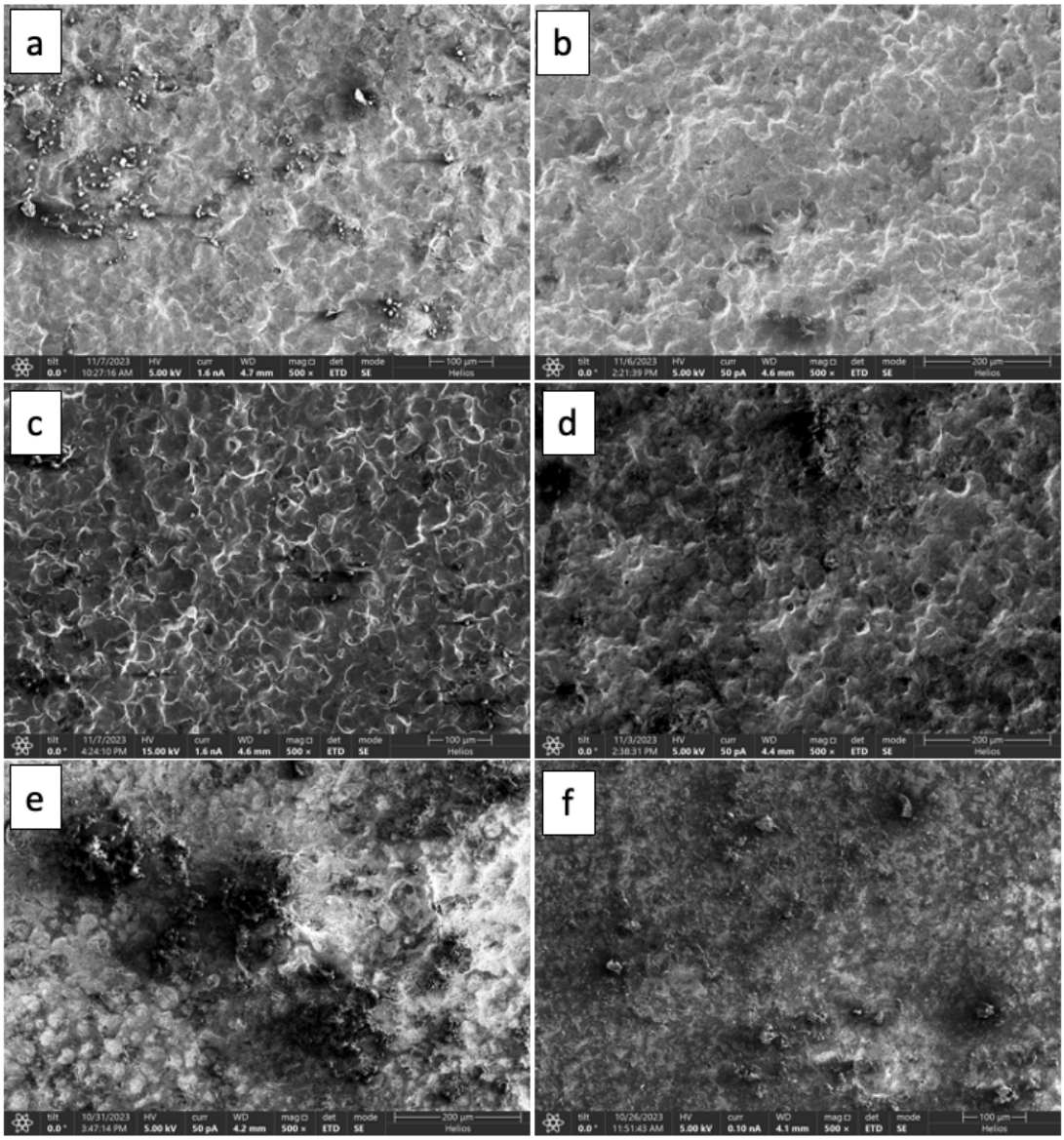

Figure 37. Top-down SEM images of each cold spray composition identified as a) Al7075 b) 10% μB_4C c) 15% μB_4C d) 20% μB_4C e) single pass 2 vol% nB_4C / 2 vol.% BNNT f) dual pass 2 vol% nB_4C / 2 vol.% BNNT

4. EDS

Energy Dispersive X-ray Spectroscopy (EDS) was conducted near the top layer of the FGC as shown in Figure 38. By detecting the X-rays emitted when a sample is bombarded with electrons, EDS provides the ability to distinguish the elemental makeup of a particular particle. Multiple spots were looked at to confirm the elemental composition.

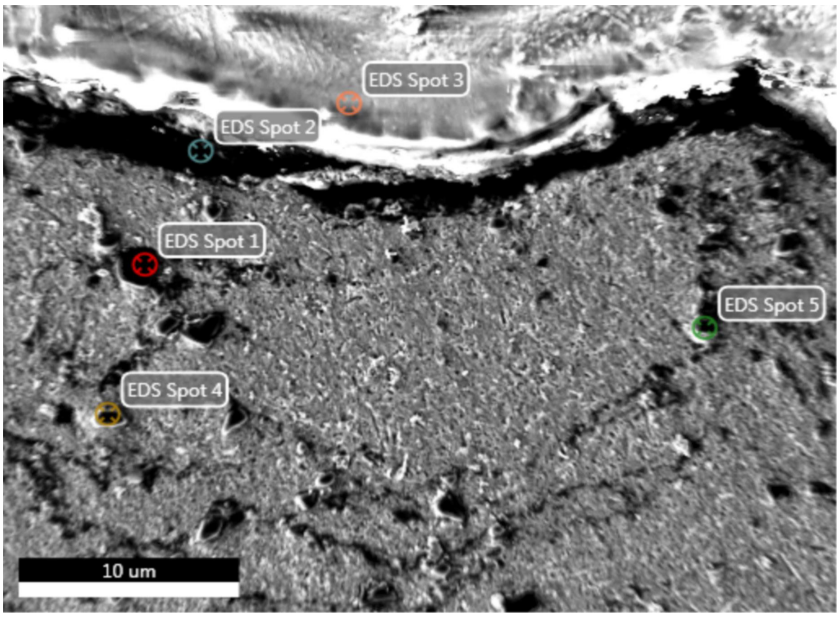

Figure 38. EDS imaging location at 2 vol% nB4C / 2 vol.% BNNT layer.

EDS Spot 1 in Figure 38 shows a μB4C particle. The size of it falls under the 1 – 3 μm size outlined by the manufacture's guidelines. As further evidence of this, seen in Figure 39, is a plot of x-ray energy in keV (abscissa) and x-ray counts (ordinate). The elemental composition is clearly composed of boron and carbon as outlined in Figure 39. Despite this analysis being qualitative, the fact that the x-ray peak corresponding to boron is elevated considerably over that of carbon further confirms the particle is in fact boron carbide. When x-ray energy is low as is the case for boron, the x-ray is more easily absorbed. So, boron x-ray counts are typically lower than expected.

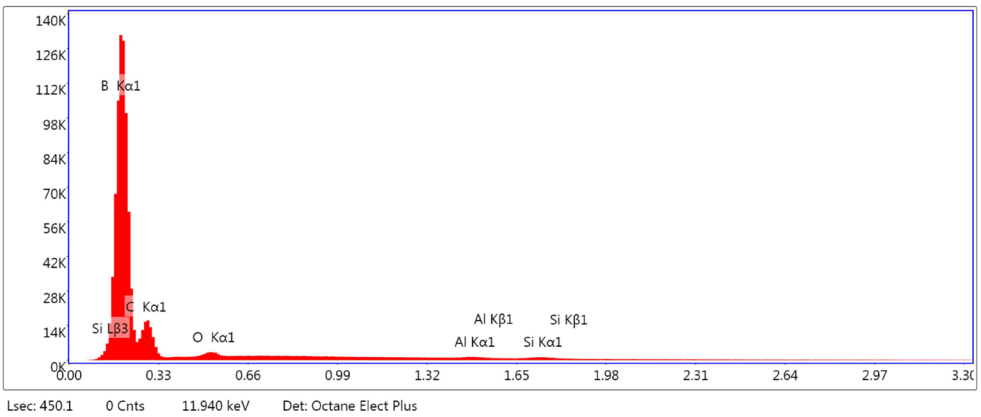

Figure 39. EDS spot 1 showing μB4C.

EDS Spots 2, 4, and 5 represent the sprayed Al7075 composite layers. The presence of a substantial amount of oxygen in this sample is likely a result of alumina residues from the polishing process. Despite thorough cleaning using supersonic cleaning methods, trace amounts of oxygen persisted throughout the sample as shown in Figure 40. EDS spot 3 was specifically targeted to confirm the presence of epoxy, revealing a composition primarily consisting of carbon with minimal oxygen.

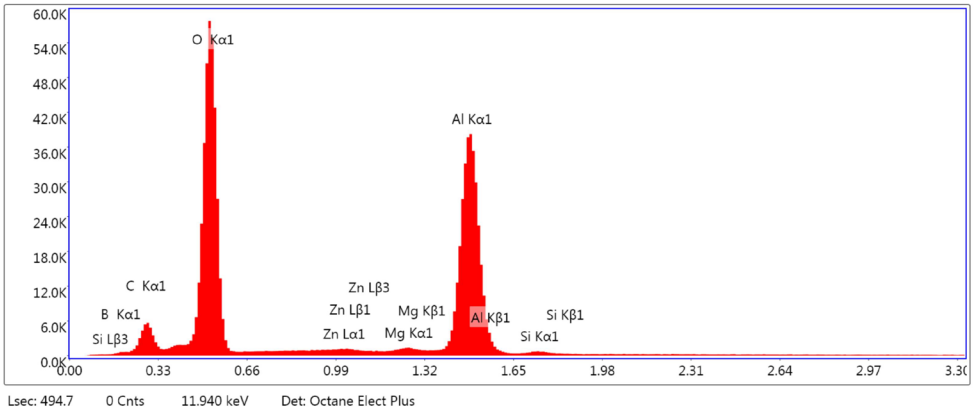

Figure 40. EDS spot 2 showing Al7075 with aluminum oxide present.

C. SURFACE PROFILE

Profilometry was used to assess the surface topography of the various FGCs before initiating wear testing. Although Al7075 was not directly utilized in the FGC, it served as

a reference for the MMC employed in this study. Multiple wear tests were conducted on each surface, and the results were averaged to determine arithmetical average roughness (Ra) and root mean squared roughness (rms) values, as illustrated in Figure 41. Throughout successive passes in the FGC, both Ra and rms values exhibited a consistent decrease.

Ra and RMS are both metrics used to quantify surface roughness. Ra represents the average deviation of the surface profile from the mean line and is calculated by averaging the absolute values of height deviations over a specified length. On the other hand, RMS measures the root mean square of the surface profile deviations, taking into account both the height and spacing of irregularities. While Ra provides a general idea of overall roughness, RMS is more sensitive to larger peaks and valleys.

The reduction was notably more pronounced when applying the 2 vol.% nB_4C / 2 vol.% BNNT. Several factors could contribute to this phenomenon: 1) the nB_4C and BNNT may have dislodged during the spray process, accelerating to an erosion velocity and thereby smoothing the 20 vol.% μB_4C layer. 2) The nB_4C and BNNT particles might have filled in the crevices present in the 20 vol.% μB_4C layer. 3) The BNNT particles may be acting as a lubricant when wear testing is being conducted. 4) A combination of both factors could be influencing the observed outcome.

The average surface values and profilometry profiles are outlined in Figure 41. They exhibit a decreasing trend with the application of each additional layer compared to the base Al7075 powder utilized.

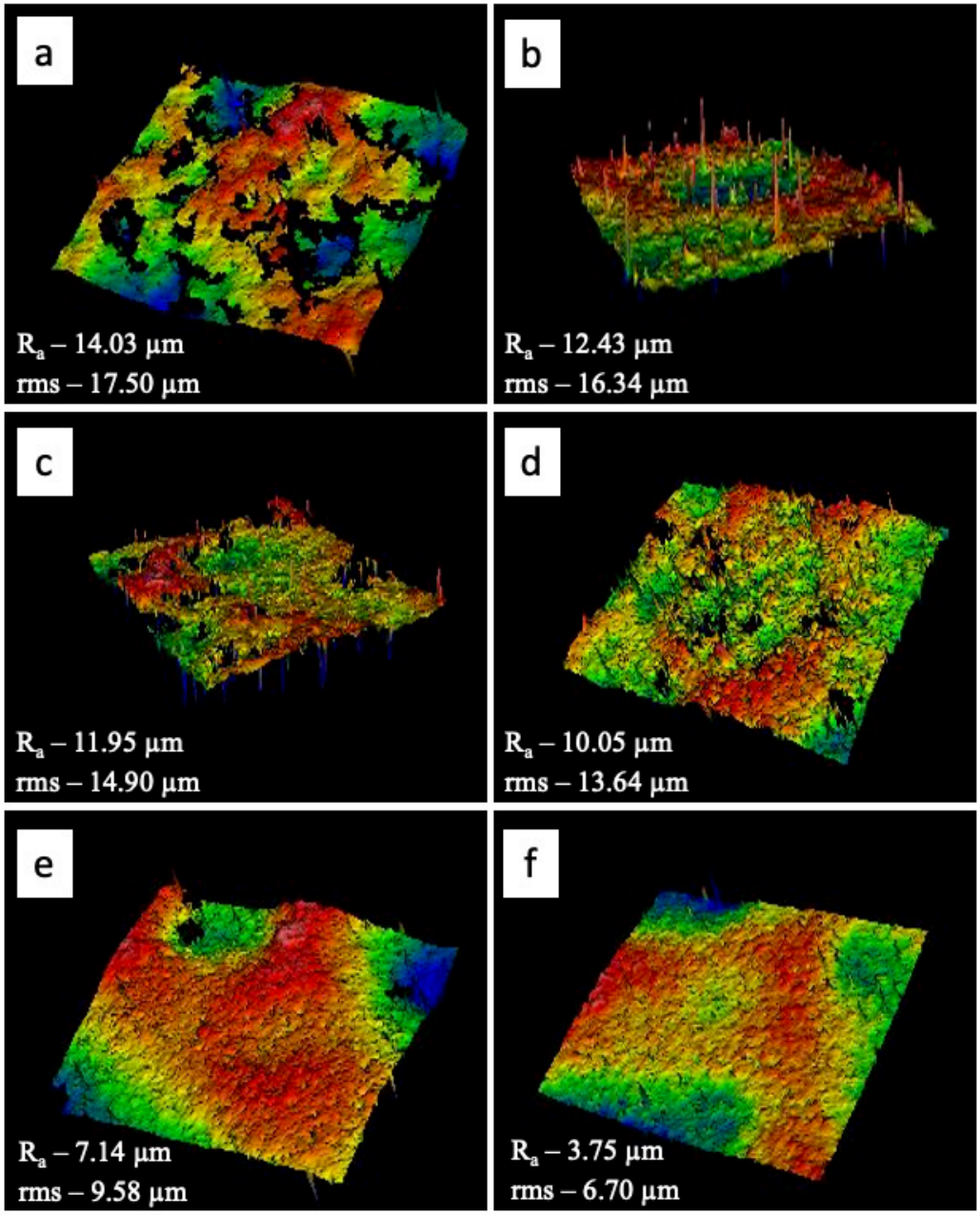

Figure 41. Surface roughness profiles identified as identified as a) Al7075 b) 10% µB_4C c) 15% µB_4C d) 20% µB_4C e) single pass 2 vol% nB_4C / 2 vol.% BNNT f) dual pass 2 vol% nB_4C / 2 vol.% BNNT

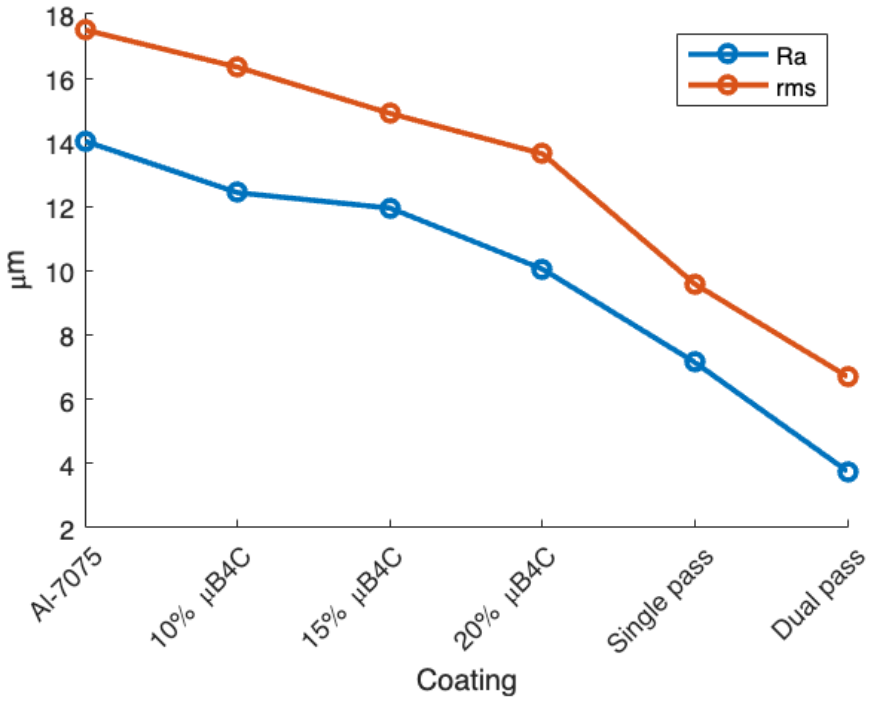

Figure 42. Surface roughness plotted with sample.

D. WEAR

During the wear testing process, the coefficient of friction (COF) for each coating was systematically recorded. Real-time COF data is visually depicted in the Appendix A. Given the inherent noise in the data collection, additional manipulation was required. A moving mean was applied to improve data clarity from the wear tester. Figure 43 displays informative data despite the presence of minor residual noise. The initial COF recorded starts at a relatively high level, trending downward thereafter. This spike is attributed to the wear tracks in the coating not fully forming, resulting in a rougher COF reading.

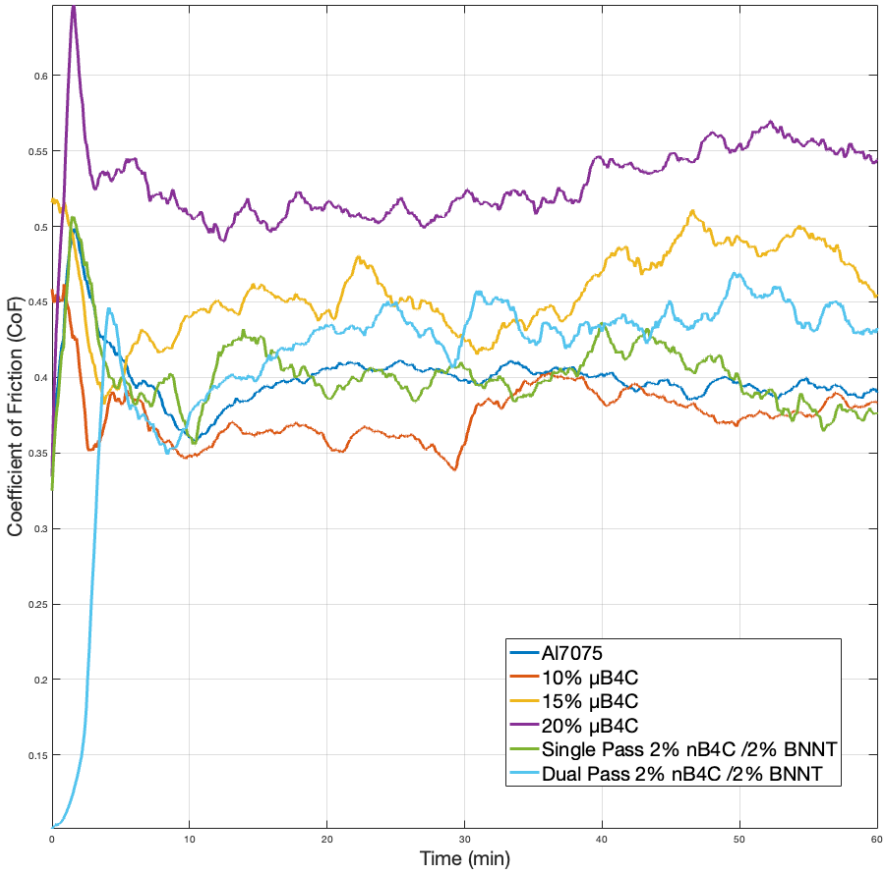

Figure 43. Coefficient of friction at 3N.

As the vol.% μB_4C increases, the COF also rises. Notably, μB_4C maintains integrity throughout the wear test. Eventually, they become dislodged as single particles, leaving gaps upon removal until the wear track progresses further down the sample. The micron-thin layers of both single pass and dual pass 2 vol.% nB_4C / 2 vol.% BNNT layers uniquely reduce the COF significantly compared to the 20 vol% μB_4C they cover. These layers, previously discussed, exhibit low adhesion characteristics due to initial breakdown on the FGC. As force is applied, these cracked pieces could further break down and partially fill in the gaps where μB_4C particles were removed.

Another consideration is that nB_4C and BNNT particles may erode the 20 vol% μB_4C layer upon application. These smaller nanometer-sized particles may be ripped off the agglomerated MMC powder in the spray nozzle, accelerating to erosion velocity based

on their size compared to the micrometer-sized Al7075 powder to which they were attached.

Wear testing was carried out each layer of the FGC as shown in Figure 26. The objective was to assess the impact of different μB_4C volume percentages (10%, 15%, and 20%) as well as the addition of 2 vol.% nB_4C and 2 vol.% BNNT layers on the overall wear resistance of each coating. As a comparison, a sprayed Al7075 coating that was made separately was included as a reference to see how the reinforcing materials complement the base Al7075 powder.

All six graded coatings underwent wear testing, with the masses of the samples recorded before and after each test to calculate the mass loss. The mass loss for each coating after completion of the 1N, 3N, and 5N wear test in the tribometer is depicted in Figure 44. The mass loss trend consistently decreased with a reduction in applied force, except for the 15% μB_4C at 3N. Additionally, there was a noticeable increase in mass loss across all three applied forces in the single and dual pass 2 vol.% nB_4C / 2 vol.% BNNT layers. This increase can be attributed to the breakdown of the layers due to low adhesion. SEM analysis revealed significant cracking in these layers, suggesting that they likely underwent removal during the wear test.

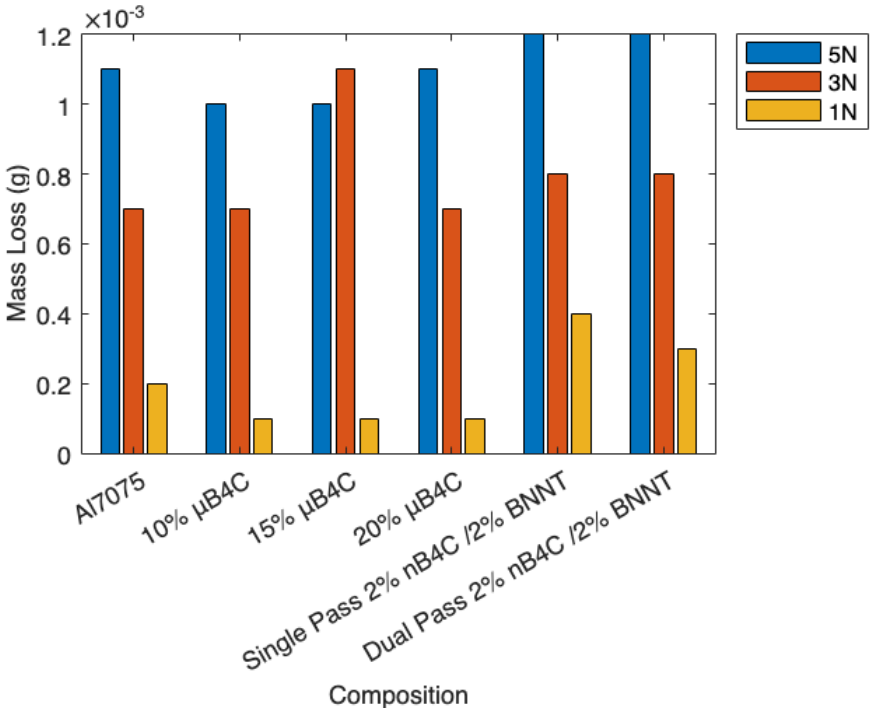

Figure 44. Mass loss after 1N, 3N, and 5N tests.

Another aspect to look at during wear testing was the depth of the encoder during the wear testing in Figure 45. Both the Al7075 and 10 vol.% μB_4C were sprayed directly onto an Al7075 substrate. The remaining passes however show a decreasing trend in depth change with each additional compositions added when a 5N load was applied as seen in Table 14.

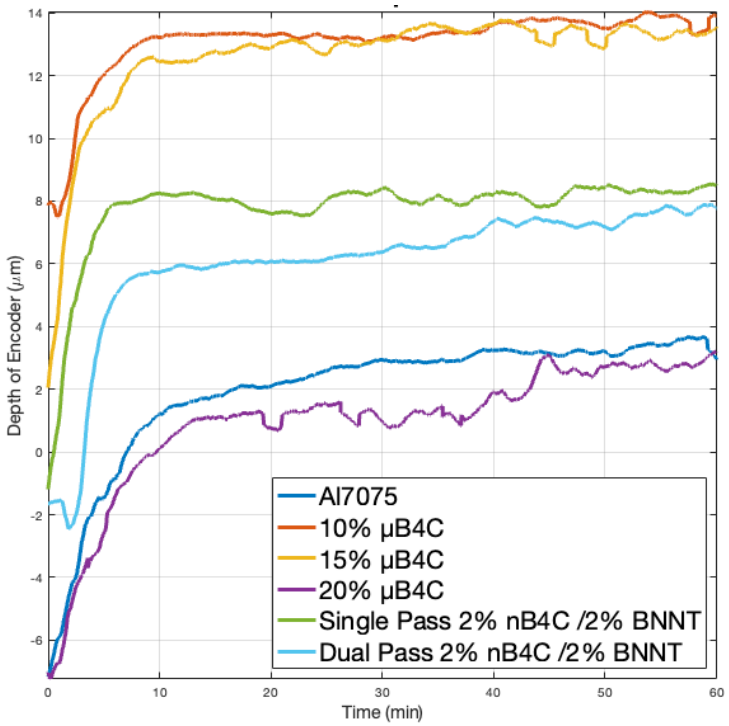

Figure 45. Tribometer encoder depth.

Table 14 and Figure 45 exhibit distinct values because of the differing reference points chosen for measurement. Figure 1 illustrates values from the commencement to the conclusion of the test, encompassing the entire duration. In contrast, Table 14 reports values derived by taking the difference between the initial depth at start and the final depth at the end of the test.

Table 14. Change of depth of encoder with 5N.

Composition	Change in Depth (μm)
Al7075	10.0821
10 vol.% μB$_4$C	6.0608
15 vol.% μB$_4$C	11.4944
20 vol.% μB$_4$C	10.1997
Single Pass	9.7076
Dual Pass	9.4300

The wear tracks formed during ball-on-disk dry sliding wear tests result from a combination of removing debris from the coating, pushing it along, and depositing it into the grooves of the wear track. Simultaneously, material is completely removed from the track.

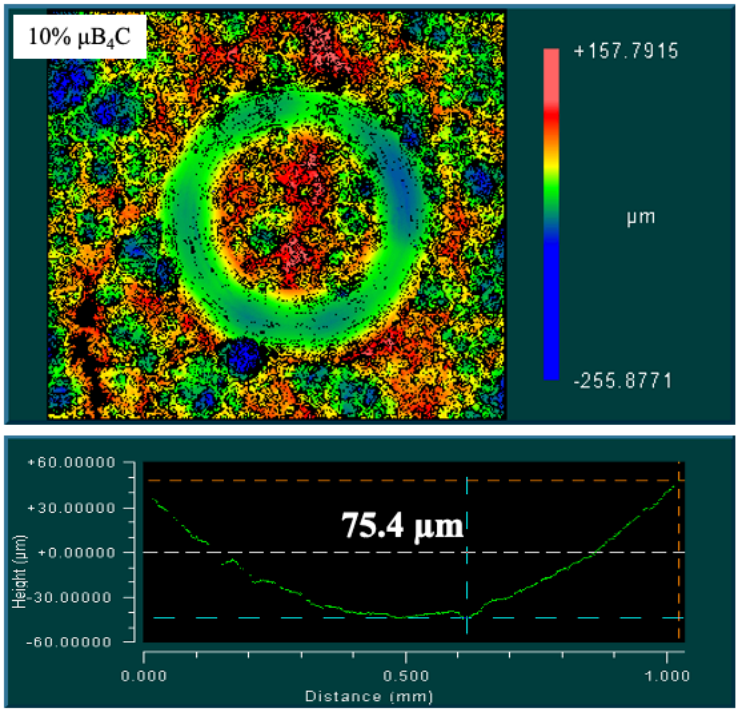

Figure 46. Optical profilometry scan of 10 vol.% µB4C (top) and depth reading (bottom).

Figure 46 illustrates an optical scan from 10 vol.% µB4C under a 5N load, and an example of its depth measurement obtained during the scan. Further measurements from a 5N load can be found in Appendix B. These depth measurements were utilized to calculate the average depth of each wear track. The compiled results allowed for the determination of the total average volume of material lost from each sample.

$$\Delta V = \frac{\pi r_t (w)^3}{6 r_b} \quad (2)$$

where r_t is the wear track radius, r_b is the radius of the ball, and w is the width of the wear track. Equation (2), a reduced approximation from ASTM G99, serves to calculate the volume loss within a disk wear track. In a comparative study utilizing a different aluminum alloy, this reduced geometrical method demonstrated differences of less than 7% when compared to a more precise method [51]. The results were subsequently computed and depicted in graphical form for different loads and compositions, as detailed in Figure 48.

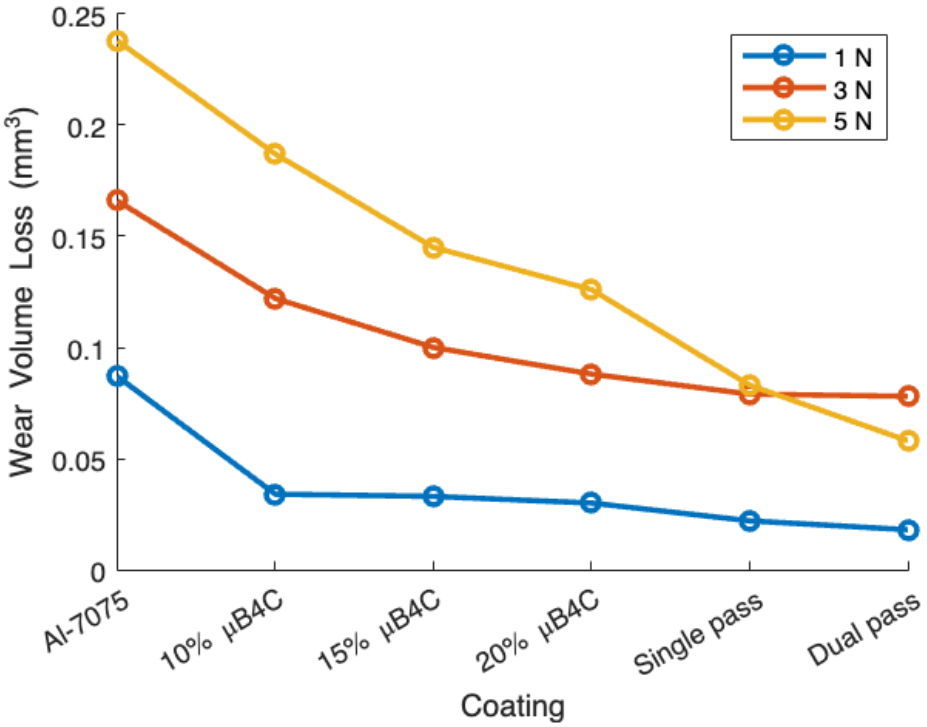

Figure 47. Wear volume loss.

$$W_s = \frac{\Delta V}{Fd} \tag{3}$$

Utilizing this information, specific wear rates (Ws) for all coatings were calculated by considering the applied force (F), total sliding distance (d), and volume (ΔV) of material lost, as outlined in Equation (2) by using Equation (3) taken from ASTM standard G99-04 [50]. Specific wear rate results are shown in Figure 48. The optical profilometry results reveal that the wear tests did not penetrate the coating. This outcome is primarily attributed

to the thickness of the coating itself. The findings from this wear test also suggest that the coatings with their ceramic reinforcements, notably improved the wear-resistant properties.

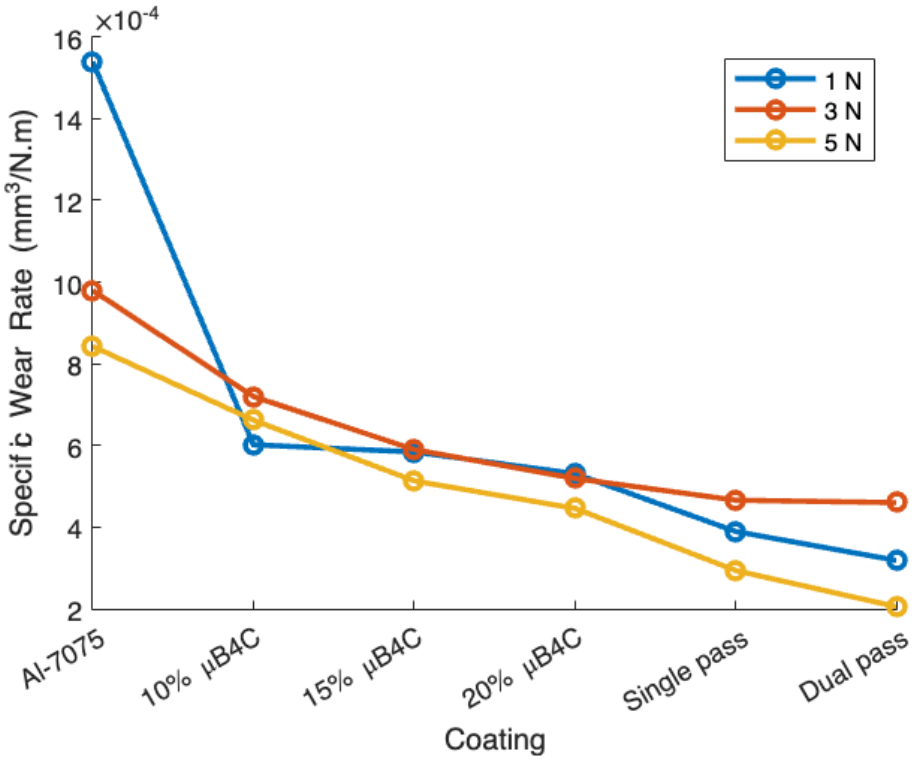

Figure 48. Specific wear rate results.

V. CONCLUSION

A. SUMMARY

This study aimed to enhance the wear resistance of Al7075 based MMC cold sprayed coatings. The Al matrix was mixed with varying amounts of nano- or micro-boron carbide and boron nitride nanotubes. Optimization of the cold spray process for these composite powders was conducted before spraying to determine the optimal combination of gas pressure, gas temperature, and other parameters. Further exploration of these parameters, however, is needed as it relates to nanosized reinforcements due to potential variations associated with size and its effects on critical velocity.

Wear resistance testing revealed that the addition of μB_4C reinforcement generally improved coating wear rates. Beyond 20% μB_4C, the deposition of MMC powder significantly decreased when paired with Al7075. Coatings reinforced with nB_4C and BNNT exhibited even lower deposition but effectively reduced wear rates through a lubricating effects associated with BNNT, or by filling in crevices with nanomaterials.

The layering of several MMCs provided a method to create a functionally graded composite (FGC). Further optimization of the cold spray process is necessary to improve coating depositions and thicknesses when spraying with the nanomaterials. Despite the challenges faced, this study establishes a solid foundation for refining compositionally graded cold spray coatings. This research, coupled with the continually advancing field of cold spray technologies, introduces an alternative repair option for the Department of Defense that can be customed tailored to specific needs.

B. RECOMMENDATIONS FOR FUTURE WORK

Incorporating small volumetric percentages of boron nitride nanotubes (BNNT) into higher boron carbide (μB_4C) compositions should be reevaluated. This addition led to a significant reduction in the clogging of the powder feed line during the spraying process. This may have the potential to improve the application process and the performance of the future coatings through this mechanism.

Further validate wear resistance, incorporating nanoindentation techniques provides a more detailed and comprehensive understanding of material properties. This advanced testing method can offer insights into the mechanical response of the coating, providing valuable data on hardness, elastic modulus, and other critical parameters that contribute to wear resistance.

Addressing the agglomeration observed in higher volumetric percentages of micro-sized boron carbide (μB_4C) involves exploring alternative mixing and separation methods. Investigating improved techniques within the powder matrix becomes essential in preventing the undesirable clumping of particles, particularly in the case of μB_4C. Enhancing mixing methods not only aids in keeping particles well-separated but also contributes to achieving better spray quality, ensuring a more uniform and effective coating application.

Powder contamination poses a significant challenge in cold spray applications, impacting the efficiency and quality of the coating deposition process. Contaminants in the powder feedstock can include foreign particles, oxides, or impurities that compromise the integrity of the sprayed coating. These contaminants can interfere with the cohesive bonding between particles during the cold spray process, leading to reduced adhesion to the substrate and diminished coating performance.

APPENDIX A: WEAR COF GRAPHS

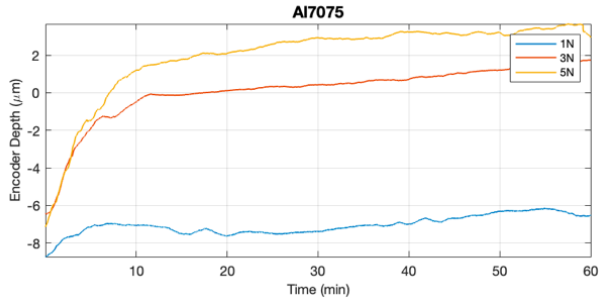

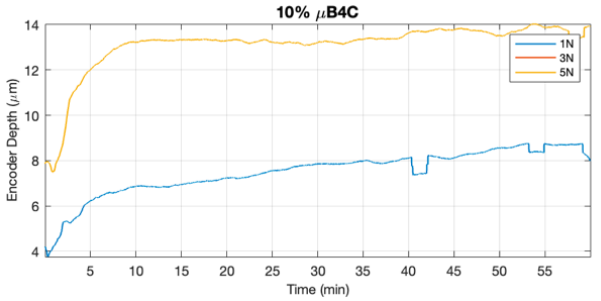

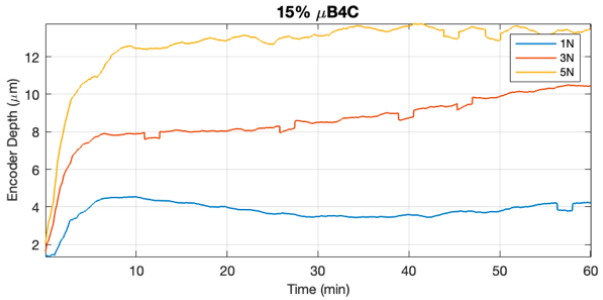

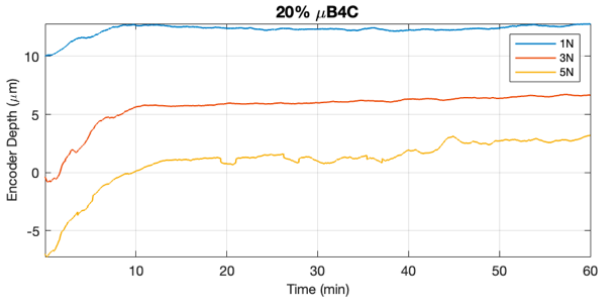

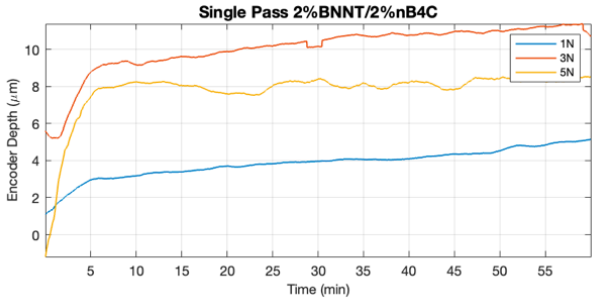

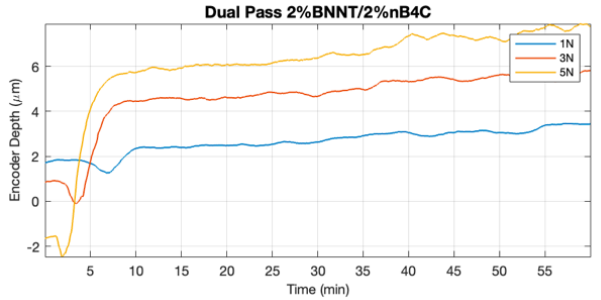

THIS PAGE INTENTIONALLY LEFT BLANK

APPENDIX B: 5N LOAD WEIGHT TEST

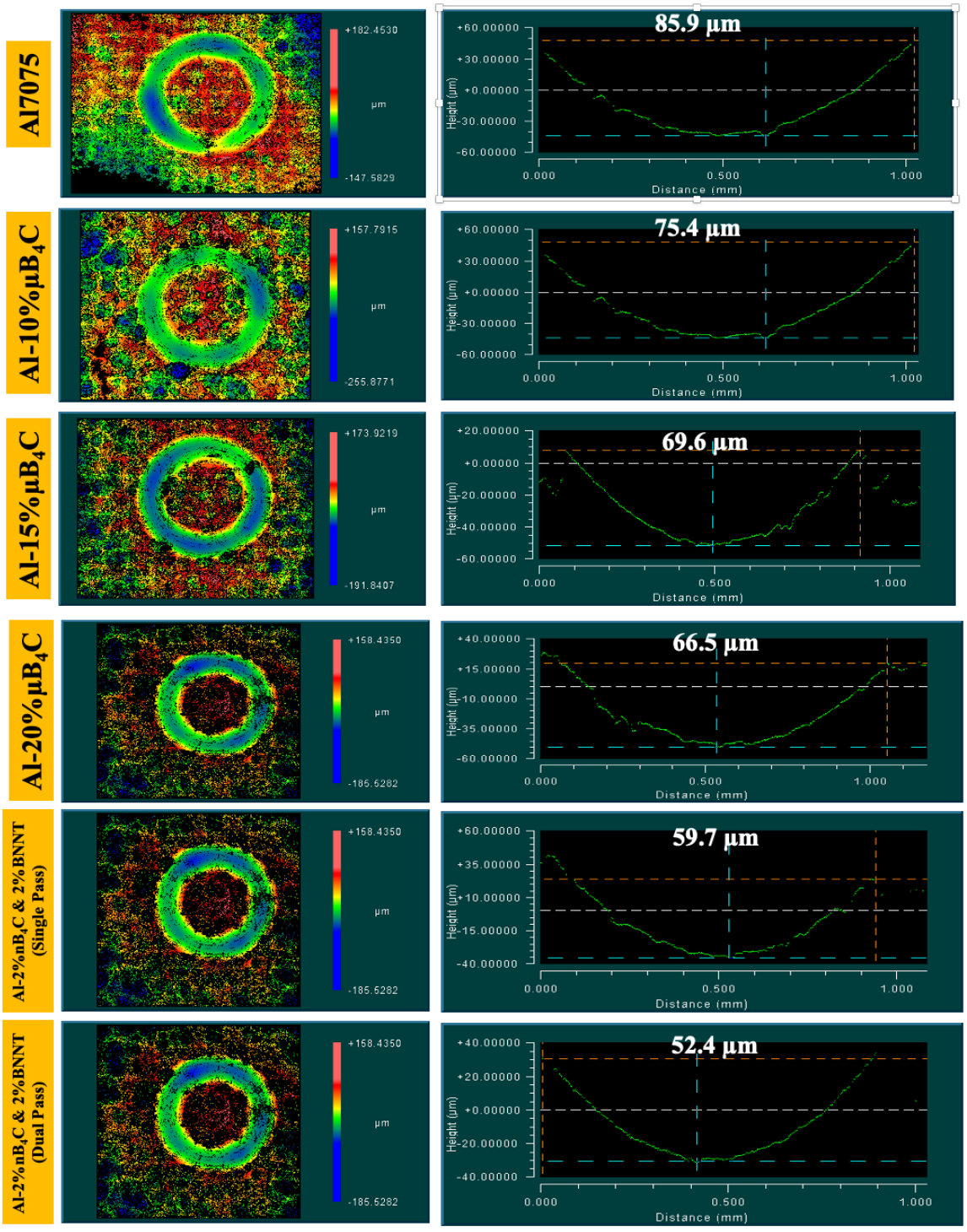

THIS PAGE INTENTIONALLY LEFT BLANK

LIST OF REFERENCES

[1] A. S. Alhulaifi and G. A. Buck, "A simplified approach for the determination of critical velocity for cold spray processes," *J. Therm. Spray Technol.*, vol. 23, pp. 1259–1269, 2014.

[2] A. Papyrin, V. Kosarev, S. Klinkov, A. Alkhimov, and V. M. Fomin, *Cold spray technology*. Elsevier, 2006.

[3] T. Schmidt *et al.*, "From particle acceleration to impact and bonding in cold spraying," *J. Therm. Spray Technol.*, vol. 18, pp. 794–808, 2009.

[4] D. Gilmore, R. Dykhuizen, R. Neiser, M. Smith, and T. Roemer, "Particle velocity and deposition efficiency in the cold spray process," *J. Therm. Spray Technol.*, vol. 8, pp. 576–582, 1999.

[5] S. P. Rice, "Enhancing mechanical properties of cold-sprayed aluminum coatings using graphene-nanoplatelet and micro-boron-carbide reinforcements." Monterey, CA; Naval Postgraduate School, Jun. 2022. Available: https://hdl.handle.net/10945/70729

[6] S. Singh, R. Raman, C. Berndt, and H. Singh, "Influence of cold spray parameters on bonding mechanisms: A review. Metals (Basel) 11 (12)," 2021.

[7] V. Champagne and D. Helfritch, "The unique abilities of cold spray deposition," *Int. Mater. Rev.*, vol. 61, no. 7, pp. 437–455, 2016.

[8] S. Pathak and G. C. Saha, "Development of sustainable cold spray coatings and 3D additive manufacturing components for repair/manufacturing applications: A critical review," *Coatings*, vol. 7, no. 8, p. 122, 2017.

[9] S. Kuroda, J. Kawakita, M. Watanabe, and H. Katanoda, "Warm spraying—a novel coating process based on high-velocity impact of solid particles," *Sci. Technol. Adv. Mater.*, 2008.

[10] S. Kumar, M. Kumar, and N. Jindal, "Overview of cold spray coatings applications and comparisons: A critical review," *World J. Eng.*, vol. 17, no. 1, pp. 27–51, 2020.

[11] T. Hussain, D. G. McCartney, P. H. Shipway, and D. Zhang, "Bonding mechanisms in cold spraying: the contributions of metallurgical and mechanical components," *J. Therm. Spray Technol.*, vol. 18, pp. 364–379, 2009.

[12] P. C. King, G. Bae, S. H. Zahiri, M. Jahedi, and C. Lee, "An experimental and finite element study of cold spray copper impact onto two aluminum substrates," *J. Therm. Spray Technol.*, vol. 19, pp. 620–634, 2010.

[13] M. Rokni, S. Nutt, C. Widener, V. Champagne, and R. Hrabe, "Review of relationship between particle deformation, coating microstructure, and properties in high-pressure cold spray," *J. Therm. Spray Technol.*, vol. 26, pp. 1308–1355, 2017.

[14] V. K. Champagne, "The Repair of Magnesium Rotorcraft Components by Cold Spray," *J. Fail. Anal. Prev.*, vol. 8, no. 2, pp. 164–175, 2008.

[15] S. Rech, A. Trentin, S. Vezzu, E. Vedelago, J.-G. Legoux, and E. Irissou, "Different cold spray deposition strategies: single-and multi-layers to repair aluminium alloy components," *J. Therm. Spray Technol.*, vol. 23, pp. 1237–1250, 2014.

[16] Q. Blochet, F. Delloro, F. N'guyen, D. Jeulin, F. Borit, and M. Jeandin, "Effect of the cold-sprayed aluminum coating-substrate interface morphology on bond strength for aircraft repair application," *J. Therm. Spray Technol.*, vol. 26, pp. 671–686, 2017.

[17] T. Stoltenhoff, H. Kreye, and H. J. Richter, "An analysis of the cold spray process and its coatings," *J. Therm. Spray Technol.*, vol. 11, pp. 542–550, 2002.

[18] K. Tsaknopoulos, B. Sousa, C. Massar, J. Grubbs, M. Siopis, and D. Cote, "A through-process experimental approach to enable optimization of cold sprayed Al 7075 consolidation performance," *JOM*, pp. 1–11, 2022.

[19] H. Koivuluoto, J. Lagerbom, M. Kylmälahti, and P. Vuoristo, "Microstructure and mechanical properties of low-pressure cold-sprayed (LPCS) coatings," *J. Therm. Spray Technol.*, vol. 17, pp. 721–727, 2008.

[20] C.-J. Li, W.-Y. Li, and H. Liao, "Examination of the critical velocity for deposition of particles in cold spraying," *J. Therm. Spray Technol.*, vol. 15, pp. 212–222, 2006.

[21] F. Gärtner, T. Stoltenhoff, T. Schmidt, and H. Kreye, "The cold spray process and its potential for industrial applications," *J. Therm. Spray Technol.*, vol. 15, pp. 223–232, 2006.

[22] O. C. Ozdemir, C. A. Widener, D. Helfritch, and F. Delfanian, "Estimating the effect of helium and nitrogen mixing on deposition efficiency in cold spray," *J. Therm. Spray Technol.*, vol. 25, pp. 660–671, 2016.

[23] D. MacDonald, S. Rahmati, B. Jodoin, and W. Birtch, "An economical approach to cold spray using in-line nitrogen–helium blending," *J. Therm. Spray Technol.*, vol. 28, pp. 161–173, 2019.

[24] T. Schmidt, F. Gaertner, and H. Kreye, “New developments in cold spray based on higher gas and particle temperatures,” *J. Therm. Spray Technol.*, vol. 15, pp. 488–494, 2006.

[25] X.-J. Ning, J.-H. Jang, and H.-J. Kim, “The effects of powder properties on in-flight particle velocity and deposition process during low pressure cold spray process,” *Appl. Surf. Sci.*, vol. 253, no. 18, pp. 7449–7455, 2007.

[26] A. Mortensen and J. Llorca, “Metal matrix composites,” *Annu. Rev. Mater. Res.*, vol. 40, pp. 243–270, 2010.

[27] D. Miracle, “Metal matrix composites–from science to technological significance,” *Compos. Sci. Technol.*, vol. 65, no. 15–16, pp. 2526–2540, 2005.

[28] B. V. Ramnath *et al.*, “Aluminium metal matrix composites–a review,” *Rev Adv Mater Sci*, vol. 38, no. 5, pp. 55–60, 2014.

[29] A. Nieto, H. Yang, L. Jiang, and J. M. Schoenung, “Reinforcement size effects on the abrasive wear of boron carbide reinforced aluminum composites,” *Wear*, vol. 390, pp. 228–235, 2017.

[30] V. Rama Koteswara Rao, N. Ramanaiah, and M. Sarcar, “Fabrication and investigation on Properties of TiC reinforced Al7075 metal matrix composites,” *Appl. Mech. Mater.*, vol. 592, pp. 349–353, 2014.

[31] S. Sardar, S. Kumar Karmakar, and D. Das, “Tribological properties of Al 7075 alloy and 7075/Al2O3 composite under two-body abrasion: a statistical approach,” *J. Tribol.*, vol. 140, no. 5, p. 051602, 2018.

[32] C. S. Koria, R. Kumar, and P. S. Chauhan, “Reinforcement of micro and nano material with aluminum alloy (Al7075) metal matrix composite: a review,” in *Journal of Physics: Conference Series*, IOP Publishing, 2023, p. 012023.

[33] I. Dowding, M. Hassani, Y. Sun, D. Veysset, K. Nelson, and C. Schuh, “Particle Size Effects in Metallic Microparticle Impact-Bonding,” *Acta Mater.*, vol. 194, May 2020, doi: 10.1016/j.actamat.2020.04.044.

[34] V. P. Mahesh, P. S. Nair, T. P. D. Rajan, B. C. Pai, and R. C. Hubli, “Processing of surface-treated boron carbide-reinforced aluminum matrix composites by liquid–metal stir-casting technique,” *J. Compos. Mater.*, vol. 45, no. 23, pp. 2371–2378, 2011.

[35] C. E. Prema, S. Suresh, G. Ramanan, and M. Sivaraj, “Characterization, corrosion and failure strength analysis of Al7075 influenced with B4C and Nano-Al2O3 composite using online acoustic emission,” *Mater. Res. Express*, vol. 7, no. 1, p. 016524, 2020.

[36] M. B. Jakubinek, K. S. Kim, M. J. Kim, A. A. Martí, and M. Pasquali, "Recent advances and perspective on boron nitride nanotubes: From synthesis to applications," *J. Mater. Res.*, vol. 37, no. 24, pp. 4403–4418, 2022.

[37] S. Kalay, Z. Yilmaz, O. Sen, M. Emanet, E. Kazanc, and M. Culha, "Synthesis of boron nitride nanotubes and their applications," *Beilstein J. Nanotechnol.*, vol. 6, no. 1, pp. 84–102, 2015.

[38] M. Ghazizadeh, J. E. Estevez, and A. D. Kelkar, "Boron nitride nanotubes for space radiation shielding," *Int J Nano Stud Technol*, vol. 4, pp. 1–2, 2015.

[39] N. P. Padture, M. Gell, and E. H. Jordan, "Thermal barrier coatings for gas-turbine engine applications," *Science*, vol. 296, no. 5566, pp. 280–284, 2002.

[40] M. Imran and A. R. A. Khan, "Characterization of Al-7075 metal matrix composites: a review," *J. Mater. Res. Technol.*, vol. 8, no. 3, pp. 3347–3356, May 2019, doi: 10.1016/j.jmrt.2017.10.012.

[41] J. M. Mistry and P. P. Gohil, "Research review of diversified reinforcement on aluminum metal matrix composites: fabrication processes and mechanical characterization," *Sci. Eng. Compos. Mater.*, vol. 25, no. 4, pp. 633–647, 2018, doi: doi:10.1515/secm-2016-0278.

[42] A. Güneş *et al.*, "Towards analysis and optimization for contact zone temperature changes and specific wear rate of metal matrix composite materials produced from recycled waste," *Materials*, vol. 14, no. 18, p. 5145, 2021.

[43] D. J. Woo *et al.*, "Synthesis of nanodiamond-reinforced aluminum metal composite powders and coatings using high-energy ball milling and cold spray," *Carbon (New York)*, vol. 63, pp. 404–415, 2013.

[44] T. Y. Ansell, T. Hanneman, A. Gonzalez-Perez, C. Park, and A. Nieto, "Effect of high energy ball milling on spherical metallic powder particulates for additive manufacturing," 2021.

[45] Solvus Global. "SAAM-AL7075-G1H1," 2023. Available: https://order.powdersondemand.com/powders/SAAM-AL7075-G1H1

[46] Us Research Nanomaterials, Inc. "Boron carbide powder / B4C powder (B4C,99.9%)," Available: https://www.us-nano.com/inc/sdetail/6703

[47] Us Research Nanomaterials, Inc. "Boron carbide b4c nanopowder / B4C nanoparticles (99+%, 45–55 nm, hexagonal)," Available: https://www.us-nano.com/inc/sdetail/6703

[48] S. Abiodun, R. Krishnamoorti, and A. K. Bhowmick, “Polytetrafluoroethylene Nanocomposites with Engineered Boron Nitride Nanobarbs for Thermally Conductive and Electrically Insulating Microelectronics and Microwave Devices,” *ACS Appl. Nano Mater.*, vol. 6, no. 5, pp. 3781–3796, 2023.

[49] D. M. Tauber, “Mechanical properties of nano boron nitride and micro boron carbide reinforced aluminum cold spray coatings.” M.S. thesis, Naval Postgraduate School, Monterey, CA, USA, Dec. 2022. Available: https://hdl.handle.net/10945/71555

[50] A. Güneş *et al.*, “Towards analysis and optimization for contact zone temperaturechanges and specific wear rate of metal matrix composite materials produced from recycled waste,” *Materials*, vol. 14, no. 18, p. 5145, Sep. 2021, doi:10.3390/ma14185145.

[51] J. Salguero, P. Iglesias, J. M. Vazquez-Martinez, M. Batista, and I. Del Sol, “A Comparative Study of Disk Wear Volume Evaluation of Al2024 Based on ASTM G99,” in *IMECE2022*, Volume 9: Mechanics of Solids, Structures, and Fluids; Micro- and Nano-Systems Engineering and Packaging; Safety Engineering, Risk, and Reliability Analysis; Research Posters, Oct. 2022. doi: 10.1115/IMECE2022-94625.

THIS PAGE INTENTIONALLY LEFT BLANK

INITIAL DISTRIBUTION LIST

1. Defense Technical Information Center
   Fort Belvoir, Virginia

2. Dudley Knox Library
   Naval Postgraduate School
   Monterey, California